
LIPSCHITZ REGULARIZED GRADIENT FLOWS AND LATENT GENERATIVE PARTICLES

Hyemin Gu*

Department of Mathematics and Statistics
University of Massachusetts
Amherst, MA 01003, USA
hgu@umass.edu

Panagiota Birmpa

Department of Actuarial Mathematics & Statistics
Heriot-Watt University
Edinburgh, EH14 4AS, U.K.
P.Birmpa@hw.ac.uk

Yannis Pantazis

Institute of Applied & Computational Mathematics
Foundation for Research & Technology - Hellas
Heraklion, Greece
pantazis@iacm.forth.gr

Luc Rey-Bellet

Department of Mathematics and Statistics
University of Massachusetts
Amherst, MA 01003, USA
luc@math.umass.edu

Markos A. Katsoulakis

Department of Mathematics and Statistics
University of Massachusetts
Amherst, MA 01003, USA
markos@umass.edu

ABSTRACT

Lipschitz regularized f -divergences are constructed by imposing a bound on the Lipschitz constant of the discriminator in the variational representation. These divergences interpolate between the Wasserstein metric and f -divergences and provide a flexible family of loss functions for non-absolutely continuous (e.g. empirical) distributions, possibly with heavy tails. We first construct Lipschitz regularized gradient flows on the space of probability measures based on these divergences. Examples of such gradient flows are Lipschitz regularized Fokker-Planck and porous medium partial differential equations (PDEs) for the Kullback-Leibler and α -divergences, respectively. The regularization corresponds to imposing a Courant–Friedrichs–Lewy numerical stability condition on the PDEs. For empirical measures, the Lipschitz regularization on gradient flows induces a numerically stable transporter/discriminator particle algorithm, where the generative particles are transported along the gradient of the discriminator. The gradient structure leads to a regularized Fisher information which is the total kinetic energy of the particles and can be used to track the convergence of the algorithm. The Lipschitz regularized discriminator can be implemented via neural network spectral normalization and the particle algorithm generates approximate samples from possibly high-dimensional distributions known only from data. Notably, our particle algorithm can generate synthetic data even in small sample size regimes. A new data processing inequality for the regularized divergence allows us to combine our particle algorithm with representation learning, e.g. autoencoder architectures. The resulting particle algorithm in latent space yields markedly improved generative properties in terms of efficiency and quality of the synthetic samples. From a statistical mechanics perspective the encoding can be interpreted dynamically as learning a better mobility for the generative particles.

*CODE

1 INTRODUCTION

In this paper we construct new algorithms that are capable of efficiently transporting arbitrary empirical distributions to a target data set. The transportation of the empirical distribution is constructed as a (discretized) gradient flow in probability space for Lipschitz-regularized f -divergences. Samples are viewed as particles and are transported along the gradient of the discriminator of the divergence towards the target data set. We take advantage of representation learning concepts, e.g. autoencoders, and make these algorithms efficient even in high-dimensional sample spaces by defining particle algorithms in latent space. Their accuracy is guaranteed by a new data processing inequality.

One of our main tools is Lipschitz regularized f -divergences which interpolate between the Wasserstein metric and f -divergences. Such divergences Dupuis & Mao (2022); Birrell et al. (2022a;c), discussed in Section 2 provide a flexible family of loss functions for non-absolutely continuous distributions. In Machine Learning one needs to build algorithms to handle target distributions Q which are singular, either by their intrinsic nature such as probability densities concentrated on low dimensional structures and/or because Q is usually only approximately known through N samples (the corresponding empirical distribution \hat{Q}_N is always singular). Another key ingredient in our construction is that we build gradient flows where mass is transported along the gradient of the optimal discriminator in the variational formulation of the divergences. The time discretization of such gradient flows for empirical distributions gives rise to a so-called transporter/discriminator particle algorithm which transports an initial empirical distribution \hat{P}_N toward the target \hat{Q}_N . The Lipschitz regularization provides numerically stable, mesh free, particle algorithms that can act as generative models for high-dimensional target distributions. Moreover the gradient structure yields a dissipation functional which corresponds to the kinetic energy of the particles (a Lipschitz regularized version of Fisher information) and which can be used to control the convergence of the algorithm. The third new element in our methods is the use of representation learning to reduce the sample space dimension. We construct latent particle algorithms by building a Lipschitz regularized gradient flow in latent space. The fidelity of the latent space particle algorithm is guaranteed by a new data processing inequality for Lipschitz regularized divergence which ensures that convergence in latent space implies convergence in real sample space.

We test and demonstrate our methods in four classes of problems. (a) Learning from synthetic data sets with heavy tails. (b) Image generation using particle algorithms even in small target sample size regimes. (c) Image-to-image transformations using latent particles. (d) Merging datasets from different breast cancer studies after transforming them using our latent particles methods aiming towards meta-analysis of gene expression data Taminau et al. (2014); Hughey & Butte (2015).

Related work. Our approach is inspired by the MMD and KALE gradient flows from Arbel et al. (2019); Glaser et al. (2021) based on an entropic regularization of the MMD metrics, and related work using the Kernelized Sobolev Discrepancy Mroueh et al. (2019). Furthermore, the recent work of Dupuis & Mao (2022); Birrell et al. (2022a) built the mathematical foundations for a large class of new divergences which contains the Lipschitz regularized f -divergences and used them to construct GANs, and in particular symmetry preserving GANs Birrell et al. (2022c)). Also related is the Sinkhorn divergence Genevay et al. (2016) which is a different entropic regularization of the 2-Wasserstein metrics. Lipschitz regularizations (or related spectral normalization) have been shown to improve the stability of GANs Miyato et al. (2018); Arjovsky et al. (2017); Gulrajani et al. (2017). Our particle algorithms share similarities with GANs Goodfellow et al. (2014); Arjovsky et al. (2017), sharing the same discriminator but having a different generator step. They are also broadly related to continuous time normalizing flows (NF) Chen et al. (2018a); Köhler et al. (2020); Chen et al. (2018b), diffusion models Sohl-Dickstein et al. (2015); Ho et al. (2020) and score-based generative flows Song & Ermon (2020); Song et al. (2021). However, the aforementioned continuous time models, along with variational autoencoders Kingma & Welling (2013) and energy based methods LeCun et al. (2006), are all likelihood-based. On the other hand, particle gradient flows such as the ones proposed here, can be classified as a separate class within implicit generative models. Within such generative models that include GANs, there is more flexibility in selecting the loss function in terms of a suitable divergence or probability metric, enabling the comparison of even mutually singular distributions, e.g. Arjovsky et al. (2017). In Section 9 we compare further

our particle methods to both GANs and other generative particles algorithms such as RKHS-based gradient flows and score-matching methods.

Gradient flows in probability spaces related to the Kullback-Leibler (KL) divergence, such as the Fokker-Planck equations and Langevin dynamics Roberts & Tweedie (1996); Durmus & Éric Moulines (2017) or Stein variational gradient descent Liu & Wang (2016); Liu (2017); Lu et al. (2019), form the basis of a variety of sampling algorithms when the target distribution Q has a known density (up to normalization). The weighted porous media equations form another family of gradient flows based on α -divergences Markowich & Villani (2000); Otto (2001); Ambrosio et al. (2005); Dolbeault et al. (2008); Vázquez (2014) which are very useful in the presence of heavy tails. Our gradient flows are Lipschitz-regularizations of such classical PDE's (Fokker-Planck and porous media equations), see Appendix 6 for a PDE and numerical analysis perspective on such flows. Finally, deterministic particle methods and associated probabilistic flows of ODEs such as the ones derived here for Lipschitz-regularized gradient flows for (f, Γ) divergences, were considered in recent works for classical KL-divergences and associated Fokker-Planck equations as sampling tools Maoutsa et al. (2020); Boffi & Vanden-Eijnden (2022), for Bayesian inference Reich & Weissmann (2021) and as generative models Song et al. (2021). Our latent generative particles approach is inspired by latent diffusion models using auto-encoders Rombach et al. (2021) and by autoencoders used for model reduction in coarse-graining for molecular dynamics, Vlachas et al. (2022); Wang & Gómez-Bombarelli (2019); Stiefenhofer et al. (2021).

Main contributions. We conclude this Section with a concise summary of the primary contributions in this paper:

- We develop an algorithm for transporting generative particles from an arbitrary source distribution to an arbitrary target distribution based on a new Lipschitz regularized gradient flow. Source and target can be mutually singular (aka non-absolutely continuous), for instance, they can both be empirical distributions corresponding to finite data. Furthermore, the use of regularized f -divergences in the form of (f, Γ) -divergences allows us to learn distributions with heavy tails from data.
- We reveal new connections with well-established results from PDEs and their numerical stability. Such as that Lipschitz regularization corresponds to imposing a Courant–Friedrichs–Lewy numerical stability condition on the (regularized) Fokker Planck PDEs.
- We extend our Lipschitz-regularized gradient flow algorithm to cover the case of transporting generative particles in the latent space. Theoretical error analysis is also provided in the form of a data processing inequality between latent and real spaces. These inequalities can serve as an *a posteriori* bound in the sense of numerical analysis, where the approximation in the tractable latent space bounds the error in the much less tractable real space.
- The proposed generative approach is validated on a wide variety of datasets and applications ranging from image generation to gene expression data integration.

The paper is structured as follows. In Section 2, we introduce the concept of (f, Γ) -divergences, their primal and dual variational representations, and discuss their interpolation between the 1-Wasserstein metric and f -divergences. In Section 3, we construct the first variation of (f, Γ) -divergences and define associated Lipschitz-regularized gradient flows in probability space. Based on such gradient flows for (f, Γ) -divergences and relying on their ability to compare mutually singular distributions, in Section 4 we define particle dynamics approximations for these flows and related time-discretized generative particle algorithms. In Section 5, we extend our Lipschitz-regularized gradient flow algorithm to latent spaces, and provide theoretical error analysis guarantees between latent and real spaces. In Section 6, we discuss new connections of Lipschitz-regularization with partial differential equations and their numerical approximations, as well as their implications for the convergence of proposed particle algorithms. In Section 7 we apply the proposed particle algorithms to low dimensional synthetic examples and high dimensional image data sets, while in Section 8 we apply our methods to a batch effects problem for gene expression data. In the context of some illustrative low-dimensional examples and the MNIST data set, in Section 9 we compare our particle methods to GANs, as well as to other generative particles algorithms such as RKHS-based gradient flows and score-matching methods. The code is available at https://github.com/HyeminGu/Lipschitz_regularized_generative_particles_algorithm.

2 LIPSCHITZ-REGULARIZED f -DIVERGENCES

In the paper Dupuis & Mao (2022), continuing with Birrell et al. (2022a) a new general class of divergences has been constructed which interpolate between f -divergences and integral probability metrics and inherit desirable properties from both. In this paper we focus on one specific family which we view as a Lipschitz regularization of the KL-divergence (or f -divergences) or as an entropic regularization of the 1-Wasserstein metric. We denote by $\mathcal{P}(\mathbb{R}^d)$ the space of all Borel probability measures on \mathbb{R}^d by $\mathcal{P}_1(\mathbb{R}^d) = \{P \in \mathcal{P}(\mathbb{R}^d) : \int |x| dP(x) < \infty\}$. We denote by $C_b(\mathbb{R}^d)$ the bounded continuous function and by $\Gamma_L = \{f : \mathbb{R}^d \rightarrow \mathbb{R} : |f(x) - f(y)| \leq L|x - y| \text{ for all } x, y\}$ the Lipschitz continuous functions with Lipschitz constant bounded by L (note that $a\Gamma_L = \Gamma_{aL}$).

f -divergences. If $f : [0, \infty) \rightarrow \mathbb{R}$ is strictly convex and lower-semicontinuous with $f(1) = 0$ the f -divergence of P with respect to Q is defined by $D_f(P||Q) = E_Q[f(\frac{dP}{dQ})]$ if $P \ll Q$ and set to be $+\infty$ otherwise. We have the variational representation (see e.g. Birrell et al. (2022a) for a proof)

$$D_f(P||Q) = \sup_{\phi \in C_b(\mathbb{R}^d)} \left\{ E_P[\phi] - \inf_{\nu \in \mathbb{R}} \{ \nu + E_Q[f^*(\phi - \nu)] \} \right\} \quad (1)$$

where $f^*(s) = \sup_{t \in \mathbb{R}} \{st - f(t)\}$ is the Legendre-Fenchel transform of f . We will use the KL-divergence with $f_{\text{KL}}(x) = x \log x$ and the α -divergence: $f_\alpha = \frac{x^\alpha - 1}{\alpha(\alpha - 1)}$ with Legendre transforms $f_{\text{KL}}^*(y) = e^{y-1}$ and $f_\alpha^* \propto y^{\frac{\alpha}{\alpha-1}}$ (see the Appendix). For KL the infimum over ν can be solved analytically and yields the Donsker-Varadhan with a $\log E_Q[e^\phi]$ term (see Birrell et al. (2022b) for more on variational representations).

Wasserstein metrics. The 1-Wasserstein metrics $W^{\Gamma_1}(P, Q)$ with transport cost $|x - y|$ is an integral probability metrics, see Arjovsky et al. (2017). By keeping the Lipschitz constant as a regularization parameter we set

$$W^{\Gamma_L}(P, Q) = \sup_{\phi \in \Gamma_L} \{E_P[\phi] - E_Q[\phi]\} \quad (2)$$

and note that we have $W^{\Gamma_L}(P, Q) = LW^{\Gamma_1}(P, Q)$.

Lipschitz-regularized f -divergences. The Lipschitz regularized f -divergences are defined directly in terms their variational representations, by replacing the optimization over bounded continuous functions in equation 1 by Lipschitz continuous functions in Γ_L .

$$D_f^{\Gamma_L}(P||Q) := \sup_{\phi \in \Gamma_L} \left\{ E_P[\phi] - \inf_{\nu \in \mathbb{R}} \{ \nu + E_Q[f^*(\phi - \nu)] \} \right\}. \quad (3)$$

Some of the important properties of Lipschitz regularized f -divergences, which summarizes results from Dupuis & Mao (2022); Birrell et al. (2022a) are given in Theorem 2.1. It is assumed there that f is super-linear (called admissible in Birrell et al. (2022a)), that is $\lim_{s \rightarrow \infty} f(s)/s = +\infty$. This excludes the case of α -divergences for $\alpha < 1$, for which the existence of optimizers is a more delicate problem, but parts of the theorems remain true.

Theorem 2.1. *Assume that f is superlinear and strictly convex. Then for $P, Q \in \mathcal{P}_1(\mathbb{R}^d)$ we have*

1. **Divergence:** $D_f^{\Gamma_L}(P||Q)$ is a divergence, i.e. $D_f^{\Gamma_L}(P||Q) \geq 0$ and $D_f^{\Gamma_L}(P||Q) = 0$ if and only if $P = Q$. Moreover the map $(P, Q) \rightarrow D_f^{\Gamma_L}(P||Q)$ is convex and lower-semicontinuous.

2. **Infimal Convolution Formula:** $D_f^{\Gamma_L}(P||Q) = \inf_{\gamma \in \mathcal{P}(\Omega)} \{W^{\Gamma_L}(P, \gamma) + D_f(\gamma||Q)\}$. In particular we have $0 \leq D_f^{\Gamma_L}(P||Q) \leq \min \{D_f(P||Q), W^{\Gamma_L}(P, Q)\}$.

3. **Interpolation and limiting behavior of $D_f^{\Gamma_L}(P||Q)$:**

$$\lim_{L \rightarrow \infty} D_f^{\Gamma_L}(P||Q) = D_f(P||Q) \quad \text{and} \quad \lim_{L \rightarrow 0} \frac{1}{L} D_f^{\Gamma_L}(P||Q) = W^{\Gamma_1}(P, Q). \quad (4)$$

4. **Optimizers:** *There exists an optimizer $\phi^{L,*} \in \Gamma_L$, unique up to a constant in $\text{supp}(P) \cup \text{supp}(Q)$.*

Remark 2.2. The optimizer $\gamma^{L,*}$ in the infimal convolution formula exists and is unique and we have $d\gamma^{L,*} \propto (f^*)'(\phi^{L,*})dQ$ (see Birrell et al. (2022a) for details). For example for KL we get $d\gamma^{L,*} \propto e^{\phi^{L,*}}dQ$.

3 LIPSCHITZ-REGULARIZED GRADIENT FLOWS AND THEIR TRANSPORTER/DISCRIMINATOR REPRESENTATION

Given a target probability distribution Q , we build an evolution equation for probability measures based on the Lipschitz regularized f -divergences $D_f^{\Gamma L}(P\|Q)$ by considering the PDE

$$\partial_t P_t = \operatorname{div} \left(P_t \nabla \frac{\delta D_f^{\Gamma L}(P\|Q)}{\delta P}(P_t) \right), \quad P_0 = P \in \mathcal{P}_1(\mathbb{R}^d) \quad (5)$$

where $\frac{\delta D_f^{\Gamma L}(P\|Q)}{\delta P}$ is the first variation of $D_f^{\Gamma L}(P\|Q)$ (to be discussed below in Theorem 3.1). An advantage of the Lipschitz regularized f -divergences is its ability to compare singular measures and so the equation 5 is to be understood in the sense of distributions (integrating against test functions).

In the limit $L \rightarrow \infty$ and if $P \ll Q$, equation 5 yields the Fokker-Planck equation (for KL divergence) and the weighted porous medium equation (for α -divergences) Otto (2001); Dolbeault et al. (2008), see Appendix 6.

The following theorem was first proved in Dupuis & Mao (2022) for KL and can be generalized to the f -divergences considered in Theorem 2.1.

Theorem 3.1. *Assume f is superlinear and strictly convex and $P, Q \in \mathcal{P}_1(\mathbb{R}^d)$.*

1. *For $x \notin \operatorname{supp}(P) \cap \operatorname{supp}(Q)$ define $\phi^{L,*}(y) = \sup_{x \in \operatorname{supp}(Q)} \{ \phi^{L,*}(x) + L|x - y| \}$ then $\phi^{L,*}$ is Lipschitz continuous on \mathbb{R}^d .*
2. *$\phi^{L,*} = \sup \{ h(x) : h \in \Gamma_L, h(y) = \phi^{L,*}(y), \text{ for every } y \in \operatorname{supp}(Q) \}$*
3. *We have*

$$\frac{\delta D_f^{\Gamma L}(P\|Q)}{\delta P}(P) = \phi^{L,*}. \quad (6)$$

In more details, let ρ be a signed measure of total mass 0 and let $\rho = \rho_+ - \rho_-$ where $\rho_{\pm} \in \mathcal{P}_1(\mathbb{R}^d)$ are mutually singular. If $P + \epsilon\rho \in \mathcal{P}_1(\mathbb{R}^d)$ for sufficiently small $|\epsilon|$ then $D_f^{\Gamma L}(P + \epsilon\rho\|Q)$ is differentiable at $\epsilon = 0$ and

$$\lim_{\epsilon \rightarrow 0} \frac{1}{\epsilon} \left(D_f^{\Gamma L}(P + \epsilon\rho\|Q) - D_f^{\Gamma L}(P\|Q) \right) = \int \phi^{L,*} d\rho. \quad (7)$$

Proof. The proof of 1. is straightforward by using the triangular inequality of norms. For 2., since $h \in \Gamma_L$, we have that $h(x) \leq h(y) + \|x - y\|$. This implies that for $y \in \operatorname{supp}(Q)$ and $x \notin \operatorname{supp}(Q)$, $h(x) \leq \inf_{y \in \operatorname{supp}(Q)} \{ h(y) + \|x - y\| \} = \inf_{y \in \operatorname{supp}(Q)} \{ \phi^{L,*}(y) + \|x - y\| \} = \phi^{L,*}(x)$. Since $\phi^{L,*}(y) \in \Gamma_L$, this concludes the proof. For 3., we use the variational formula equation 3 for $D_f^{\Gamma L}(P + \epsilon\rho\|Q)$ where we suppose that $P + \epsilon\rho \in \mathcal{P}_1(\mathbb{R}^d)$.

$$\begin{aligned} D_f^{\Gamma L}(P + \epsilon\rho\|Q) &= \sup_{\phi \in \Gamma_L} \left\{ E_{P+\epsilon\rho}[\phi] - \inf_{\nu \in \mathbb{R}} \{ \nu + E_Q[f^*(\phi - \nu)] \} \right\} \\ &\geq \int \phi^{*,L} d(P + \epsilon\rho) - \inf_{\nu \in \mathbb{R}} \left\{ \nu + \int f^*(\phi^{*,L} - \nu) dQ \right\} \\ &= \epsilon \int \phi^{*,L} d\rho + D_f^{\Gamma L}(P\|Q) \end{aligned} \quad (8)$$

Thus

$$\liminf_{\epsilon \rightarrow 0^+} \frac{1}{\epsilon} \left(D_f^{\Gamma L}(P + \epsilon\rho\|Q) - D_f^{\Gamma L}(P\|Q) \right) \geq \int \phi^{*,L} d\rho$$

For the other direction: Let us define $F(\epsilon) = D_f^{\Gamma L}(P + \epsilon\rho\|Q)$. By Theorem 18 and 71 in Birrell et al. (2022a), $F(\epsilon)$ is convex, lower semicontinuous and finite on $[0, \epsilon_0]$. Due to the convexity of F , F is differentiable on $(0, \epsilon_0)$ except for a countable number of points. Let $\epsilon \in (0, \epsilon_0)$ such that F is differentiable and $\delta > 0$ small. Also, let $\phi_\epsilon^{*,L}$ be the optimizer of $D_f^{\Gamma L}(P + \epsilon\rho\|Q)$ satisfying $\phi_\epsilon^{*,L}(0) = 0$ so that

$$D_f^{\Gamma L}(P + \epsilon\rho\|Q) = \int \phi_\epsilon^{*,L} d(P + \epsilon\rho) - \inf_{\nu \in \mathbb{R}} \left\{ \nu + \int f^*(\phi_\epsilon^{*,L} - \nu) dQ \right\}$$

By using the same argument as before in the proof, we have that

$$D_f^{\Gamma L}(P + (\epsilon + \delta)\rho\|Q) - D_f^{\Gamma L}(P + \epsilon\rho\|Q) \geq \delta \int \phi_\epsilon^{*,L} d\rho \quad (9)$$

and

$$D_f^{\Gamma L}(P + (\epsilon - \delta)\rho\|Q) - D_f^{\Gamma L}(P + \epsilon\rho\|Q) \geq -\delta \int \phi_\epsilon^{*,L} d\rho \quad (10)$$

which gives us that

$$\begin{aligned} \int \phi_\epsilon^{*,L} d\rho &\leq \lim_{\delta \rightarrow 0} \frac{1}{\delta} \left(D_f^{\Gamma L}(P + (\epsilon + \delta)\rho\|Q) - D_f^{\Gamma L}(P + \epsilon\rho\|Q) \right) \\ &= F'(\epsilon) \\ &= \lim_{\delta \rightarrow 0} \frac{1}{\delta} \left(D_f^{\Gamma L}(P + \epsilon\rho\|Q) - D_f^{\Gamma L}(P + (\epsilon - \delta)\rho\|Q) \right) \\ &\leq \int \phi_\epsilon^{*,L} d\rho \end{aligned} \quad (11)$$

Consequently,

$$F'(\epsilon) = \int \phi_\epsilon^{*,L} d\rho \quad (12)$$

Let $F'_+(0) = \lim_{\epsilon \rightarrow 0^+} \frac{1}{\epsilon} (F(\epsilon) - F(0))$. By convexity, for any sequence $\{\epsilon_n\}_{n \in \mathbb{N}}$ such that $\epsilon_0 > \epsilon_n \downarrow 0$, we have

$$F'_+(0) = \lim_{n \rightarrow \infty} F'(\epsilon_n) = \lim_{n \rightarrow \infty} \int \phi_{\epsilon_n}^{*,L} d\rho$$

By applying the Arzelá-Ascoli to $\phi_{\epsilon_n}^{*,L}$, and then doing a diagonalization argument, there exists a subsequence of $\{n_k\}_{k \geq 0} \subset \{n\}_{n \geq 0}$, such that $\phi_{\epsilon_{n_k}}^{*,L}$ converges pointwise to a function $\phi_0^{*,L} \in \text{Lip}^L(\mathbb{R}^d)$. For simplicity, from now on we denote n the convergent subsequence.

At this point, we recall that for any $\epsilon \in (0, \epsilon_0)$, $\phi_\epsilon^{*,L}(0) = 0$. For any x , $|\phi_\epsilon^{*,L}(x) - \phi_\epsilon^{*,L}(0)| \leq L\|x\|_d$ which implies that

$$|\phi_\epsilon^{*,L}(x)| \leq L\|x\|_d$$

Thus by the dominated convergence theorem

$$F'_+(0) = \lim_{n \rightarrow \infty} \int \phi_{\epsilon_n}^{*,L} d\rho = \int \phi_0^{*,L} d\rho$$

By the lower semicontinuity of $D_f^{\Gamma L}(\cdot\|Q)$, we have

$$\begin{aligned} D_f^{\Gamma L}(P\|Q) &\leq \liminf_{n \rightarrow \infty} D_f^{\Gamma L}(P + \epsilon_n\rho\|Q) \\ &= \liminf_{n \rightarrow \infty} \left\{ E_{P + \epsilon_n\rho}[\phi_{\epsilon_n}^{*,L}] - \inf_{\nu \in \mathbb{R}} \{ \nu + E_Q[f^*(\phi_{\epsilon_n}^{*,L} - \nu)] \} \right\} \\ &= \liminf_{n \rightarrow \infty} E_{P + \epsilon_n\rho}[\phi_{\epsilon_n}^{*,L}] - \limsup_{n \rightarrow \infty} \inf_{\nu \in \mathbb{R}} \{ \nu + E_Q[f^*(\phi_{\epsilon_n}^{*,L} - \nu)] \} \\ &\leq E_P[\phi_0^{*,L}] - \inf_{\nu \in \mathbb{R}} \{ \nu + E_Q[f^*(\phi_0^{*,L} - \nu)] \} \\ &\leq D_f^{\Gamma L}(P\|Q) \end{aligned} \quad (13)$$

where for the second inequality we use the dominated convergence theorem, equation 12 and that by Fatou's lemma

$$\limsup_{n \rightarrow \infty} \int \phi_{\epsilon_n}^{*,L} dQ \geq \liminf_{n \rightarrow \infty} \int \phi_{\epsilon_n}^{*,L} dQ \geq \int \phi_0^{*,L} dQ$$

Since both sides of the inequality coincide, $\phi_0^{*,L}$ must be the optimizer. By Theorem 3.1, part 1. and part 2., we have that $\phi_0^{*,L}(x) \leq \phi^{*,L}$ for all x . Thus

$$F'_+(0) = \int \phi_0^{*,L} d\rho \leq \int \phi^{*,L} d\rho.$$

which concludes the proof. \square

Combining Theorem 3.1 with equation 5 leads to a new class of PDEs:

Transporter/Discriminator PDE:

$$\partial_t P_t = \operatorname{div}(P_t \nabla \phi_t^{L,*}), \quad \text{where } \phi_t^{L,*} = \arg \max_{\phi \in \Gamma_L} \{E_{P_t}[\phi] - E_Q[f^*(\phi)]\} \quad (14)$$

Remark 3.2. **(a)** The transporter/discriminator PDE equation 14 makes sense when P and Q are replaced by their empirical measures \hat{P}_N, \hat{Q}_N based on N IID samples. This will be the basis of our numerical algorithm in Section 4 (see Algorithm 1). **(b)** Also equation 14 makes sense if P and Q are mutually singular (e.g. when Q is supported on a low-dimensional structure). We can view equation 14 as a Lipschitz regularization of classical PDEs which allows particle-based approximations based on data. In particular, the Lipschitz condition on $\phi \in \Gamma_L$ enforces a finite speed of propagation of at most L in the transport equation in equation 14. This is in sharp contrast with the Fokker Planck equation given in Appendix 6 which is a diffusion equation, see Appendix 6.2 for more details and practical implications.

4 LIPSCHITZ-REGULARIZED GENERATIVE PARTICLES

In this section we build a numerical algorithm to solve the transporter/discriminator gradient flow when N IID samples from the target distribution are given. For a map $T : \mathbb{R}^d \rightarrow \mathbb{R}^d$ and $P \in \mathcal{P}(\mathbb{R}^d)$, the pushforward measure is denoted by $T_{\#}P$ (i.e. $T_{\#}P(A) = P(T^{-1}(A))$). The forward-Euler discretization of the system equation 14 yields:

Euler method for the Transporter/Discriminator PDE:

$$P_{n+1} = (I - \Delta t \nabla \phi_n^{L,*})_{\#} P_n, \quad \text{where } \phi_n^{L,*} = \arg \max_{\phi \in \Gamma_L} \{E_{P_n}[g] - E_Q[f^*(\phi)]\} \quad (15)$$

When only N IID samples $\{X^{(i)}\}_{i=1}^N$ of the target distribution Q are available we build a particle system by considering N IID samples $\{Y^{(i)}\}_{i=1}^N$ from some initial measure P ($M \neq N$ samples are also possible) and equation 15 becomes

Lipschitz regularized generative particles:

$$Y_{n+1}^{(i)} = Y_n^{(i)} - \Delta t \nabla \phi_n^{L,*}(Y_n^{(i)}), \quad \phi_n^{L,*} = \arg \max_{\phi \in \Gamma_L} \left\{ \frac{\sum_{i=1}^N \phi(Y_n^{(i)})}{N} - \frac{\sum_{i=1}^N f^*(\phi(X^{(i)}))}{N} \right\} \quad (16)$$

The empirical measure $\hat{P}_n^N = N^{-1} \sum_{i=1}^N \delta_{Y_n^{(i)}}$ built from equation 16 gives a solution of the system equation 15 if we use as target the empirical measure $\hat{Q}^N = N^{-1} \sum_{i=1}^N \delta_{X^{(i)}}$ and as initial condition the empirical measure $\hat{P}_0^N = N^{-1} \sum_{i=1}^N \delta_{Y_0^{(i)}}$.

Remark 4.1. **(a)** The transport mechanism given by equation 16 is linear. However, nonlinear interactions between particles as introduced via the discriminator $\hat{\phi}_n^{L,*}$ are created due to the velocity field $\nabla \phi_n^{L,*}$ which depends on all particles that comprise \hat{P}_n^N and \hat{Q}^N at each step n . **(b)** Computationally, the discriminator optimization (over Lipschitz continuous functions) is implemented, for example, via spectral normalization for neural networks architectures. Moreover the gradient of the discriminator is computed only at the positions of the particles. **(c)** The Lipschitz bound L on

Algorithm 1: Lipschitz regularized generative particles algorithm

Require: f defined in equation 2 and its Legendre conjugate f^* , L : Lipschitz constant, T : number of updates for the particles, γ : time step size, N : number of particles

Require: $W = \{W^l\}_{l=1}^D$: parameters for the neural network $\phi : \mathbb{R}^d \rightarrow \mathbb{R}$, D : depth of the neural network, δ : learning rate of the neural network, T_{NN} : number of updates for the neural network.

Result: $\{Y_T^{(i)}\}_{i=1}^N$

- 1 Sample $\{X^{(i)}\}_{i=1}^N \sim Q$, a batch from the real data
- 2 Sample $\{Y_0^{(i)}\}_{i=1}^N \sim P_0 = P$, a batch of prior samples
- 3 Initialize W randomly and $W^l \leftarrow L^{1/D} * W^l / \|W^l\|_2$
- 4 **for** $n = 0$ **to** $(T - 1)$ **do**
- 5 **for** $m = 0$ **to** $T_{\text{NN}} - 1$ **do**
- 6 $grad_W \leftarrow \nabla_W \left[N^{-1} \sum_{i=1}^N \phi(Y_n^{(i)}; W) - N^{-1} f^*(\phi(X_n^{(i)}; W)) \right]$
- 7 $W \leftarrow W + \delta * grad_W$
- 8 $W^l \leftarrow L^{1/D} * W^l / \|W^l\|_2$
- 9 **end**
- 10 $Y_{n+1}^{(i)} \leftarrow Y_n^{(i)} - \gamma \nabla \phi_n^L(Y_n^{(i)}; W), \quad i = 1, \dots, N$
- 11 **end**

the discriminator space implies a pointwise bound $|\nabla \phi_n^{L,*}(Y_n^{(i)})| \leq L$ and thus the particle speed is bounded by L . Hence the Lipschitz regularization imposes a speed limit L on the particles, ensuring the stability of the algorithm for suitable choices of L . This implicit grid is reminiscent of the Courant, Friedrichs, and Lewy (CFL) condition for the stability of discrete scheme. These are fundamental features for the performance and the stability of Algorithm 1 derived from equation 16 (see Sections 7) and Appendix 6.

Kinetic energy of particles: The gradient structures implies, see Theorem 6.1, that, for equation 14, the derivative of the regularized divergence satisfies $\frac{d}{dt} D_f^{\Gamma L}(P_t \| Q) = -I_f^{\Gamma L}(P_t \| Q)$ where $I_f^{\Gamma L}(P_t \| Q) = E_{P_t} [|\nabla \phi^{L,*}|^2]$ which is interpreted as a Lipschitz-regularized Fisher Information. As $L \rightarrow \infty$ one recovers for example the Fisher Information used for the Fokker-Planck equation. For the Algorithm 1 the Lipschitz-regularized Fisher information

$$I_f^{\Gamma L}(\hat{P}_n^N \| \hat{Q}^N) = \int |\nabla \phi_n^{L,*}|^2 \hat{P}_n^N(dx) = \frac{1}{N} \sum_{i=1}^N |\nabla \phi_n^{L,*}(Y_n^{(i)})|^2, \quad (17)$$

is equal to the total kinetic energy of the particle since $\nabla \phi_n^{L,*}(Y_n^{(i)})$ is the velocity of the i^{th} particle at time n . Clearly when the total kinetic energy $I_f^{\Gamma L}(\hat{P}_n^N \| \hat{Q}^N)$ is zero, the algorithm will stop.

5 LATENT GENERATIVE PARTICLES: GRADIENT FLOWS IN LATENT SPACE

A standard paradigm of machine learning is that target measures are often supported on low dimensional structures. We leverage this insight, in the form of an auto-encoder, to construct particle algorithms in a latent, lower dimensional, space. The resulting latent particle algorithms are both more accurate and efficient, even in high-dimensional sample spaces, and their performance is guaranteed by a new Data Processing Inequality in Theorem 5.1.

Latent space model with encoder and decoder maps. Assume $Q = Q^{\mathcal{Y}}$ is supported on some low dimensional set $S \subset \mathcal{Y} = \mathbb{R}^d$, an encoder map $\mathcal{E} : \mathcal{Y} \rightarrow \mathcal{Z}$ where $\mathcal{Z} \subset \mathbb{R}^{d'}$, $d' < d$ and a decoder map $\mathcal{D} : \mathcal{Z} \rightarrow \mathcal{Y}$ are invertible in S , i.e. $\mathcal{D} \circ \mathcal{E}(S) = \mathcal{D}(\mathcal{Z}) = S$. We denote by $\mathcal{E}_{\#} Q^{\mathcal{Y}}$ the image of the measure $Q^{\mathcal{Y}}$ by the map \mathcal{E} , i.e. for $A \subset \mathcal{Z}$, we define $\mathcal{E}_{\#} Q^{\mathcal{Y}}(A) = Q^{\mathcal{Y}}(\mathcal{E}^{-1}(A))$ and likewise for $\mathcal{D}_{\#} P^{\mathcal{Z}}$. The following theorem expresses how information remains controlled under encoding/decoding and guarantees the performance of the approximation $\mathcal{D}_{\#} P^{\mathcal{Z}}$ in the real space.

The latter is achieved by an *a posteriori* estimate (18), in the sense of numerical analysis, where the approximation in the tractable latent space \mathcal{Z} will bound the error in the real space \mathcal{Y} .

Theorem 5.1. *Suppose that*

1. **Perfect encoding.** *For $Q^{\mathcal{Y}}$ the encoder \mathcal{E} and the decoder \mathcal{D} are such that $\mathcal{D}_{\#}\mathcal{E}_{\#}Q^{\mathcal{Y}} = Q^{\mathcal{Y}}$.*
2. **Lipschitz decoder.** *The decoder is Lipschitz continuous with Lipschitz constant $a_{\mathcal{D}}$.*

Then, for any $P^{\mathcal{Z}} \in \mathcal{P}_1(\mathcal{Z})$ we have

$$D_f^{\Gamma_L}(\mathcal{D}_{\#}P^{\mathcal{Z}}\|Q^{\mathcal{Y}}) \leq D_f^{\Gamma_{a_{\mathcal{D}}L}}(P^{\mathcal{Z}}\|\mathcal{E}_{\#}Q^{\mathcal{Y}}). \quad (18)$$

Remark 5.2. In practice an auto-encoder is trained on data using the empirical measure \hat{Q}_N and suitable loss function and neural network architectures. Assumption 2 in Theorem 5.1 can easily be enforced using e.g. spectral normalization. Assumption 1 is a reasonable, but somewhat idealized, version of the requirement that the autoencoder captures adequately the features of the dataset Q . In particular the dimension of the latent space \mathcal{Z} needs to be selected carefully (see Section 7).

We generalize the encoding/decoding maps to encoding/decoding probability kernels in the following paragraph. Then we prove the general version theorem 5.4 of the Theorem 5.1 which is a consequence of a new, tighter data processing inequality in Theorem 5.3 derived in Birrell et al. (2022a) that involves both transformations of probabilities and discriminator spaces Γ .

Latent space model with encoder and decoder probability kernels. The encoder map $\mathcal{E} : \mathcal{Y} \rightarrow \mathcal{Z}$ (for instance $\mathcal{Y} = \mathbb{R}^d$, $\mathcal{Z} \subset \mathbb{R}^{d'}$, $d' \ll d$) and a decoder map $\mathcal{D} : \mathcal{Z} \rightarrow \mathcal{Y}$ can be identified as dirac kernels $K_{\mathcal{E}}(y, dz) = \delta_{\mathcal{E}(y)}(dz)$ and $K_{\mathcal{D}} = \delta_{\mathcal{D}(z)}(dy)$.

1. A pullback function induced by the kernel $K_{\mathcal{E}}$ is given as

$$K_{\mathcal{E}}[f](y) := \int f(z')K_{\mathcal{E}}(y, dz') = f(\mathcal{E}(y)) \quad (19)$$

for $f \in \mathcal{M}_b(\mathcal{Z})$, $y \in \mathcal{Y}$

2. A push-forward measure induced by the kernel $K_{\mathcal{E}}$ maps $\mathcal{P}(\mathcal{Y}) \rightarrow \mathcal{P}(\mathcal{Z})$ and defines a push-forward measure which is given as

$$K_{\mathcal{E}}[P](B) := \int K_{\mathcal{E}}(y, B)P(dy) = P \circ \mathcal{E}^{-1}(B) \quad (20)$$

for $P \in \mathcal{P}(\mathcal{Y})$ and a \mathcal{Z} -measurable set B .

Likewise, the kernel $K_{\mathcal{D}}$ induces a pullback function and a push-forward measure in the opposite direction. In the previous formulation, the $Q^{\mathcal{Y}}$ -perfect encoding property $\mathcal{D}_{\#}\mathcal{E}_{\#}Q^{\mathcal{Y}} = Q^{\mathcal{Y}}$ can be rewritten as $Q^{\mathcal{Y}} = K_{\mathcal{D}}[K_{\mathcal{E}}[Q^{\mathcal{Y}}]]$. Given any $P^{\mathcal{Y}} \in \mathcal{P}(\mathcal{Y})$, we have the latent probability measure $P^{\mathcal{Z}} = K_{\mathcal{E}}[P^{\mathcal{Y}}] \in \mathcal{P}(\mathcal{Z})$ and the reconstructed probability measure $\tilde{P}^{\mathcal{Y}} = K_{\mathcal{D}}[K_{\mathcal{E}}[P^{\mathcal{Y}}]] \in \mathcal{P}(\mathcal{D}(\mathcal{Z}))$ where $\mathcal{D}(\mathcal{Z}) \subset \mathcal{Y} = \mathbb{R}^d$. In general, $\tilde{P}^{\mathcal{Y}} \neq P^{\mathcal{Y}}$.

General transition probability kernels are defined in the form of conditional distributions: $K_p(y, dz) = p(dz|y)$ from \mathcal{Y} to \mathcal{Z} and $K_q(z, dy) = q(dy|z)$ from \mathcal{Z} to \mathcal{Y} . The kernel-induced pullback functions $K_p[f](y) = \int f(z')p(dz'|y) = \mathbb{E}_{Z|Y=y \sim p(dz|y)}[f(Z)|Y = y]$ or $K_q[g](z) = \int f(y')q(dy'|z) = \mathbb{E}_{Y|Z=z \sim q(dy|z)}[g(Y)|Z = z]$ are interpreted as conditional expectations. In addition, the kernels induce push forward measures $P^{\mathcal{Z}}(dz) = p(dz|y)P^{\mathcal{Y}}(dy)$ for $P^{\mathcal{Y}} \in \mathcal{P}(\mathbb{R}^d)$ or $R^{\mathcal{Y}}(dy) = q(dy|z)R^{\mathcal{Z}}(dz)$ for $R^{\mathcal{Z}} \in \mathcal{P}(\mathbb{R}^{d'})$. For the Q -perfect encoding property, we require these kernels to satisfy $dQ^{\mathcal{Y}}(dy) = q(dy|z)p(dz|y)dQ^{\mathcal{Z}}(dz)$.

Theorem 5.3 (Data processing inequality for (f, Γ) -divergences). *Given a real valued convex function f , $P, Q \in \mathcal{P}(\Omega)$, and a probability kernel K from (Ω, \mathcal{M}) to (N, \mathcal{N}) , if $\Gamma \subset \mathcal{N}$ is nonempty, then*

$$D_f^{\Gamma}(K[P]\|K[Q]) \leq D_f^{K[\Gamma]}(P\|Q). \quad (21)$$

Proof. From the variational formulation of divergences, we have

$$D_f^\Gamma(K[P]||K[Q]) = \sup_{\phi \in \Gamma, \nu \in \mathbb{R}} \int \int (\phi(y) - \nu) K(x, dy) P(dx) - \int \int f^*(\phi(y) - \nu) K(x, dy) Q(dx). \quad (22)$$

Since f^* is convex, Jensen's inequality gives

$$\int f^*(\phi(y) - \nu) K(x, dy) \geq f^* \left(\int (\phi(y) - \nu) K(x, dy) \right) \quad (23)$$

for all $x \in \Omega$. Hence,

$$D_f^\Gamma(K[P]||K[Q]) \leq \sup_{\phi \in \Gamma, \nu \in \mathbb{R}} \mathbb{E}_P[K[\phi] - \nu] - \mathbb{E}_Q[f^*(K[\phi] - \nu)] = D_f^{K[\Gamma]}(P||Q). \quad (24)$$

□

Now we state and prove the Theorem 5.1 using the encoding/decoding probability kernels.

Theorem 5.4. *Suppose that*

1. **Perfect encoding.** *For $Q^{\mathcal{Y}}$ the encoder \mathcal{E} and decoder \mathcal{D} are such that $K_{\mathcal{D}}[K_{\mathcal{E}}[Q^{\mathcal{Y}}]] = Q^{\mathcal{Y}}$.*
2. $K_{\mathcal{D}}[\Gamma_{\mathcal{Y}}] \subset \Gamma_{\mathcal{Z}}$. *The pullback functions induced by the decoder kernel is included in the real function space.*

Then, for any $P^{\mathcal{Z}} \in \mathcal{P}(\mathbb{R}^{d'})$ we have

$$D_f^{\Gamma_{\mathcal{Y}}}(K_{\mathcal{D}}[P^{\mathcal{Z}}]||Q^{\mathcal{Y}}) \leq D_f^{\Gamma_{\mathcal{Z}}}(P^{\mathcal{Z}}||K_{\mathcal{E}}[Q^{\mathcal{Y}}]). \quad (25)$$

Proof. Since the encoder \mathcal{E} and the decoder \mathcal{D} perfectly reconstruct $Q^{\mathcal{Y}}$,

$$D_f^{\Gamma_{\mathcal{Y}}}(K_{\mathcal{D}}[P^{\mathcal{Z}}]||Q^{\mathcal{Y}}) = D_f^{\Gamma_{\mathcal{Y}}}(K_{\mathcal{D}}[P^{\mathcal{Z}}]||K_{\mathcal{D}}[K_{\mathcal{E}}[Q^{\mathcal{Y}}]]).$$

From data processing inequality,

$$D_f^{\Gamma_{\mathcal{Y}}}(K_{\mathcal{D}}[P^{\mathcal{Z}}]||K_{\mathcal{D}}[K_{\mathcal{E}}[Q^{\mathcal{Y}}]]) \leq D_f^{K_{\mathcal{D}}[\Gamma_{\mathcal{Y}}]}(P^{\mathcal{Z}}||K_{\mathcal{E}}[Q^{\mathcal{Y}}]).$$

By the assumption that $K_{\mathcal{D}}[\Gamma_{\mathcal{Y}}] \subset \Gamma_{\mathcal{Z}}$,

$$D_f^{K_{\mathcal{D}}[\Gamma_{\mathcal{Y}}]}(P^{\mathcal{Z}}||K_{\mathcal{E}}[Q^{\mathcal{Y}}]) \leq D_f^{\Gamma_{\mathcal{Z}}}(P^{\mathcal{Z}}||K_{\mathcal{E}}[Q^{\mathcal{Y}}]).$$

□

Remark 5.5. Assumption 2 in Theorem 5.4 is the generalized version of the assumption 2 in Theorem 5.1. i.e. $K_{\mathcal{D}}[\Gamma_{\mathcal{Y}}] \subset \Gamma_{\mathcal{Z}}$ for Lipschitz continuous function space $\Gamma_{\mathcal{Y}}$ can be achieved by having a Lipschitz continuous decoder \mathcal{D} .

Gradient flow in latent spaces. If $\phi_t^{\mathcal{Z}}$ is the discriminator in latent space leading to the gradient flow (14), $\partial_t P_t^{\mathcal{Z}} = \text{div}(P_t^{\mathcal{Z}} \nabla \phi_t^{\mathcal{Z}})$ then, in the particle algorithm, each particle is transported following (the time-discretization of) the ODE $\dot{z}_t = -\nabla \phi_t^{\mathcal{Z}}(z_t)$, as in Section 4. See the Algorithm 2. Upon decoding we find the transport ODE in real space is

$$\dot{y}_t = \left(\frac{\partial \mathcal{D}}{\partial z}(z_t) \right)^T \dot{z}_t = - \left(\frac{\partial \mathcal{D}}{\partial z}(z_t) \right)^T \frac{\partial \mathcal{D}}{\partial z}(z_t) \nabla_y \phi_t^{\mathcal{Y}}(\mathcal{D}(z_t)) \quad (26)$$

where $\frac{\partial \mathcal{D}}{\partial z}(z_t)$ is the Jacobian of \mathcal{D} at the point z_t and the reconstructed discriminator $\phi^{\mathcal{Y}}$ is given by $\phi^{\mathcal{Z}} = \phi^{\mathcal{Y}} \circ \mathcal{D}$. Using (26) we can therefore interpret the encoding as learning a mobility $\mu_t = \frac{\partial \mathcal{D}}{\partial z}(z_t)^T \frac{\partial \mathcal{D}}{\partial z}(z_t)$, i.e., learning a better geometry in real space. This leads to a gradient flow in real space with non-trivial mobility, cf. (14),

$$\partial_t P_t^{\mathcal{Y}} = \text{div}(\mu_t P_t^{\mathcal{Y}} \nabla \phi_t^{\mathcal{Y}}). \quad (27)$$

Algorithm 2: Latent Lipschitz regularized generative particles algorithm

Require: f defined in equation 2 and its Legendre conjugate f^* , L : Lipschitz constant, T : number of updates for the particles, γ : time step size, N : number of particles

Require: $W = \{W^l\}_{l=1}^D$: parameters for the neural network $\phi : \mathbb{R}^{d'} \rightarrow \mathbb{R}$, D : depth of the neural network, δ : learning rate of the neural network, T_{NN} : number of updates for the neural network.

Require: $\mathcal{E} : \mathbb{R}^d \rightarrow \mathbb{R}^{d'}$: trained encoder, $\mathcal{D} : \mathbb{R}^{d'} \rightarrow \mathbb{R}^d$: trained decoder.

Result: $\{Y_T^{(i)}\}_{i=1}^N$

- 1 Sample $\{\bar{X}^{(i)} = \mathcal{E}(X^{(i)}) \in \mathbb{R}^{d'}\}_{i=1}^N$ where $\{X^{(i)}\} \sim Q$ is a batch from the real data
 - 2 Sample $\{\bar{Y}_0^{(i)} = \mathcal{E}(Y^{(i)}) \in \mathbb{R}^{d'}\}_{i=1}^N$ where $\{Y^{(i)}\} \sim P_0 = P$ is a batch of prior samples
 - 3 Apply Lipschitz regularized generative particles algorithm 1 on $\bar{X}^{(i)}$ and $\bar{Y}_0^{(i)}$
 - 4 Reconstruct $Y_T^{(i)} = \mathcal{D}(\bar{Y}_T^{(i)})$
-

We note that the mobility concept is well-known in computational materials science where it is used to model kinetics of species and interfaces, see for instance Cahn (1965); Zhu et al. (1999); Wang et al. (2020). Finally, we note a similar computation to (26) in Mroueh et al. (2019) regarding the interpretation of GAN's as a gradient flow. The differences (and similarities) between (Lipschitz-regularized) Generative particle algorithm (GPA) and GAN are summarized in Figure 1 and Table 1, where in the latter we also include a comparison between mobilities.

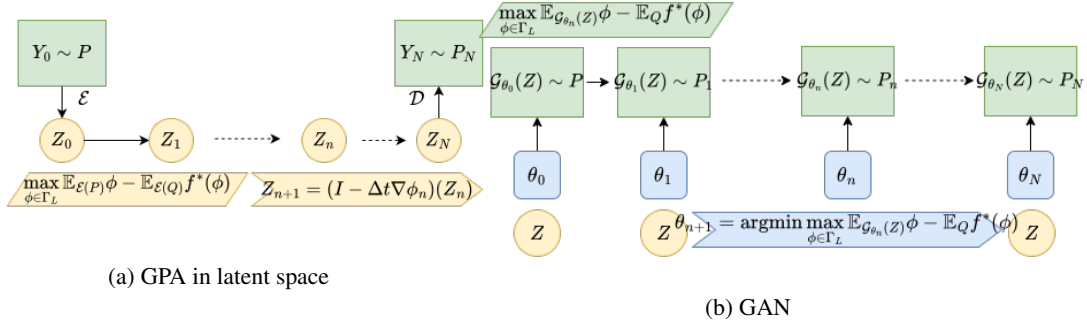


Figure 1: Workflow of different generative models. green: real space, yellow: latent space, blue: parameter space

	GPA	GPA in a latent space	GAN
Discriminator	$\phi^{\mathcal{Y}} \in \text{Lip}(\mathcal{Y})$	$\phi^{\mathcal{Z}} \in \text{Lip}(\mathcal{Z})$	$\phi^{\mathcal{Y}} \in \text{Lip}(\mathcal{Y})$
Generator	$(I_{\mathcal{Y}} - \Delta t \nabla \phi^{\mathcal{Y}})_{\#} P_n^{\mathcal{Y}}$	$(\mathcal{D} \circ (I_{\mathcal{Z}} - \Delta t \nabla \phi^{\mathcal{Z}}))_{\#} P_n^{\mathcal{Z}}$	$\mathcal{G}_{\theta}(z), z \sim \mathcal{N}(\mathbf{0}, I_{\mathcal{Z}})$
Updates	Particles $y \in \mathcal{Y}$	Particles $z \in \mathcal{Z}$	Generator parameters $\theta \in \mathbb{R}^{ \theta }$
Mobility μ , (27)	$I_{\mathcal{Y}}$	$\frac{\partial \mathcal{D}}{\partial z}(z_t)^T \frac{\partial \mathcal{D}}{\partial z}(z_t)$	$\frac{\partial \mathcal{G}(\theta_t, z)}{\partial \theta}^T \frac{\partial \mathcal{G}(\theta_t, z)}{\partial \theta}$

Table 1: Comparison of features in GPA, GPA in the latent space and GAN. $\mathcal{Y} = \mathbb{R}^d$ and $\mathcal{Z} = \mathcal{E}(\mathcal{Y})$.

6 PDE, CONVERGENCE & LEARNING RATES

Here, we discuss how PDE perspectives and tools provide insights for the analysis, stability and convergence for the proposed generative particle algorithms. We focus on continuous time for convenience. By recalling Theorem 2.1, part 4. and $\gamma^{L,*} \rightarrow P$ as $L \rightarrow \infty$ (if P is absolutely continuous with respect to Q) in Remark 2.2, equation 14 becomes a Lipschitz-regularized f -divergences gra-

dent flow (with its limit as $L \rightarrow \infty$), i.e.

$$\underbrace{\partial_t P_t = \operatorname{div} \left(P_t \nabla f' \left(\frac{d\gamma^{L,*}}{dQ} \right) \right)}_{\text{Lip. regularized } f\text{-divergence flow}} \xrightarrow{L \rightarrow \infty} \underbrace{\partial_t P_t = \operatorname{div} \left(P_t \nabla f' \left(\frac{dP_t}{dQ} \right) \right)}_{f\text{-divergence flow}} \quad (28)$$

The right hand side of equation 28 is a nonlinear operator which encodes the Lipschitz regularization in the discriminator space. This defines a new class of PDE gradient flows where absolute continuity between P_t and Q for every $t \geq 0$, is not required, contrary to gradient flows of f -divergences (obtained as $L \rightarrow \infty$.) We discuss these connections next in the context of two well-known PDEs, the (linear) Fokker-Planck and the (non-linear) porous media equation. Rewriting the limiting equation in terms of the density $h_t = \frac{dP_t}{dQ}$ we have

1. Lipschitz-regularized Fokker-Planck. For the KL, $f(x) = x \log(x)$ we obtain

$$\partial_t P_t = \operatorname{div} \left(P_t \nabla \log \left(\frac{d\gamma_t^{\Gamma L,*}}{dQ} \right) \right) \xrightarrow{L \rightarrow \infty} \partial_t h_t = (\Delta + \nabla \log(q) \cdot \nabla) h_t \quad (29)$$

2. Lipschitz-regularized Weighted Porous Medium equation (WPME). For the α -divergence with $f_\alpha(x) = \frac{1}{\alpha(\alpha-1)} x^\alpha$ we obtain a regularization of the porous media equation Otto (2001); Dolbeault et al. (2008)

$$\partial_t P_t = \frac{1}{\alpha-1} \operatorname{div} \left(p_t \nabla \left(\frac{\eta_t^{\Gamma L,*}}{q} \right)^{\alpha-1} \right) \xrightarrow{L \rightarrow \infty} \partial_t h_t = \frac{1}{\alpha} (\Delta + \nabla \log q \cdot \nabla) h_t^\alpha \quad (30)$$

6.1 CONVERGENCE TO EQUILIBRIUM AND FUNCTIONAL INEQUALITIES

Functional inequalities are fundamental methods for guaranteeing the convergence of gradient flow PDE to their equilibrium states and therefore are natural tools for studying convergence properties for the corresponding particle-based algorithms. A first step is to compute the rate of change of the divergence along solutions P_t of equation 14.

Theorem 6.1. [Lipschitz regularized dissipation] *Along a trajectory of a smooth solution $\{P_t\}_{t \geq 0}$ of equation 14 with source probability distribution P we have the following rate of decay identity:*

$$\frac{d}{dt} D_f^{\Gamma L}(P_t \| Q) = -I_f^{\Gamma L}(P_t \| Q) \leq 0 \quad (31)$$

where we define the Lipschitz-regularized Fisher Information as

$$I_f^{\Gamma L}(P \| Q) = \int |\nabla \phi^{L,*}|^2 P(dx) = E_P \left[\left| \nabla f' \left(\frac{d\gamma^{L,*}}{dQ} \right) \right|^2 \right]. \quad (32)$$

Consequently, for any $T \geq 0$, we have $D_f^{\Gamma L}(P_T \| Q) = D_f^{\Gamma L}(P \| Q) - \int_0^T I_f^{\Gamma L}(P_s \| Q) ds$.

Remark 6.2. **(a)** For the generative particles the Lipschitz-regularized Fisher Information can be interpreted as their total kinetic energy, see Paragraph 11. **(b)** When $f = f_{\text{KL}}$, as $L \rightarrow \infty$, we recover the usual Fisher information $I_f^\Gamma(P \| Q) = E_P \left[\left| \nabla \log \left(\frac{p}{q} \right) \right|^2 \right]$ which is used to prove convergence to the equilibrium state for the Fokker-Planck equation 29.

Functional inequalities, such as the classical Poincaré and the Logarithmic Sobolev-type inequalities, and many generalizations thereof see Markowich & Villani (2000); Otto & Villani (2000); Toscani & Villani (2000); Dolbeault et al. (2008); Wang (2005) are a powerful to prove convergence to equilibrium (e.g exponential or polynomial convergence), building on dissipation estimates such as Theorem 6.1. For example, if for some $\lambda > 0$, a Sobolev inequality $D_f^\Gamma(P \| Q) \leq \frac{1}{\lambda} I_f^\Gamma(P \| Q)$ holds (true when Q is sub-Gaussian), then we obtain exponential convergence to Q for any P_0 : $D_f^\Gamma(P_t \| Q) \leq e^{-\lambda t} D_f^\Gamma(P_0 \| Q)$. There exists various results, e.g. Carrillo et al. (2006); Dolbeault et al. (2008); Markowich & Villani (2000); Wang (2008), reviewed in the Section A, B, on functional inequalities when $L = \infty$ which have been used to prove convergence to equilibrium (at exponential or polynomial rate) for Fokker-Planck and/or the porous media equation when the target distribution are Gaussian distribution, stretched exponential and Student- t type distribution. The existence of functional inequalities for Lipschitz-regularized gradient flows is an open question.

6.2 NUMERICAL ANALYSIS FOR LIPSCHITZ REGULARIZED PDES AND GENERATIVE PARTICLES

For a Lipschitz-regularized gradient flow equation 28, the transporter/discriminator representation equation 14 implies that the domain of dependence is determined by the velocity fields $\nabla\phi_t^{L,*}$ whose norm is bounded by the Lipschitz constant L . Therefore the domain of dependence of the solution is finite and is contained in a cone of slope L that emanates from any point (x, t) back to the time plane $t = 0$.

From a numerical analysis point of view, equation 15 is an explicit numerical scheme $\frac{p_{n+1}-p_n}{\Delta t} = \text{div}(p_n \nabla\phi_n^{L,*}(x))$. For corresponding spatial discretization schemes there is an abundance of numerical methods which we can use to get some numerical analysis insight into our particle schemes equation 15. In particular, the Courant, Friedrichs, and Lewy (CFL) condition for stability of discrete schemes asserts that a numerical method can be convergent only if its numerical domain of dependence contains the true domain of dependence of the continuous PDE, LeVeque (2007). In our context, the CFL condition means $\sup_x |\nabla\phi_t^{L,*}(x)| \frac{\Delta t}{\Delta x} \leq C_{max}$ where $C_{max} = 1$ for such explicit schemes, LeVeque (2007). Clearly, the Lipschitz regularization enforces a CFL type condition with a learning rate Δt proportional to the inverse of L . It remains an open question how to rigorously extend this CFL analysis to particle-based algorithms where the spatial discretization grid Δx is known only implicitly as noted in Remark 4.1(b), see also related questions in Carrillo et al. (2017). Nevertheless, in our experiments we explore the inversely proportional relation between L and Δt suggested by the CFL analysis.

7 EXPERIMENTS

Transportation of particles through our Lipschitz regularized f -divergence flows involves several aspects to be discussed along with experiments.

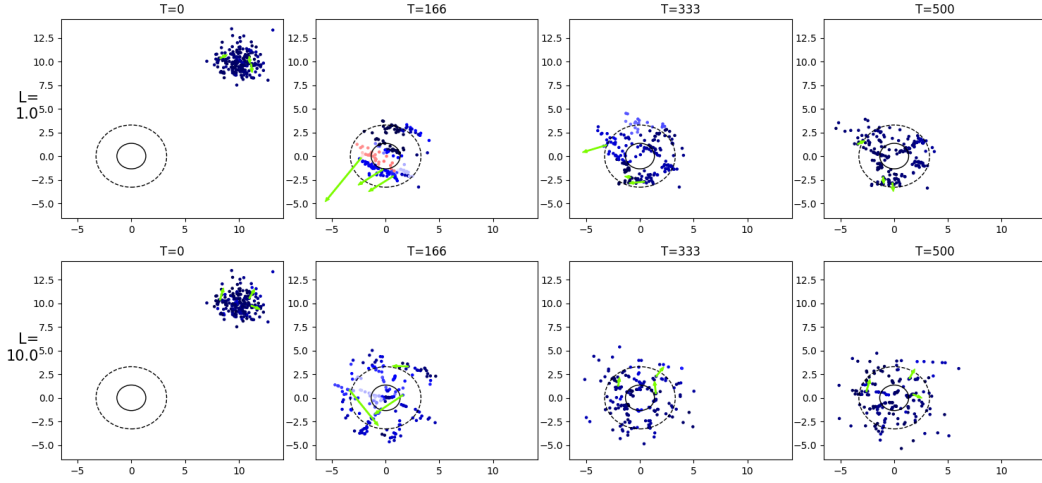
First, we explore the choice of f in order to obtain the appropriate objective functions depending on the target distribution. In addition, the Lipschitz regularization parameter L plays an important role in the stability of the propagation of particles. In subsection 7.1, we show the numerical evidence that the stability of the GPA depends on the choice of f especially for heavy-tailed distributions such as *Student*- $t(0.5)$. The supporting analytical statements are available for the classical KL-divergence flow and α -divergence flow in Appendix A and B, respectively. Also we show the numerical stability of GPA with respect to the choice of L .

In addition, once we use GPA for image generation, we can come up with different sub-problems such as conditional generation and image-to-image transformation. We note that we do not constrain (the analytical form of) the source distribution to be transported. Moreover, our algorithm can be trained using a small number of target data. In Section 7.2, we explore conditional generation and image transform tasks on MNIST data set in a small target sample size regime.

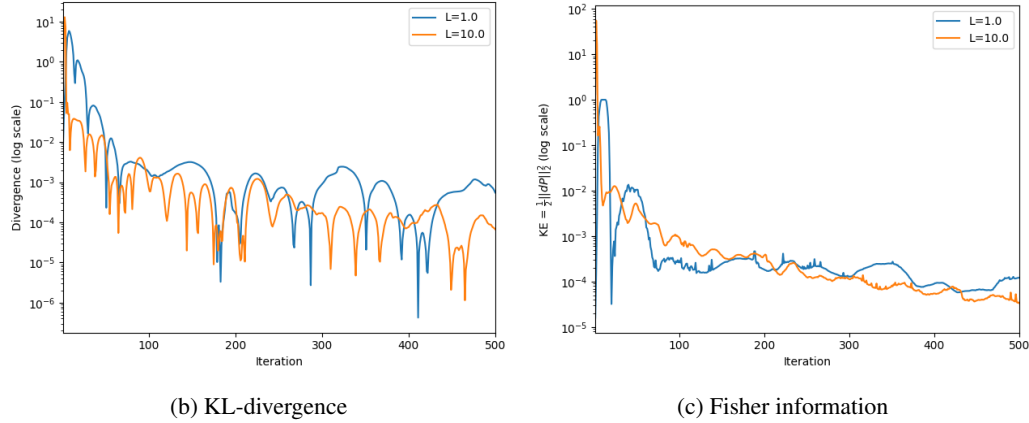
7.1 LOW DIMENSIONAL EXAMPLES WITH DIFFERENT TAILS

Our low dimensional examples illustrate the interplay between the Lipschitz regularization parameter L which stabilizes the propagation of particles and the choice of divergences f to capture the tail behavior of the target Q . We have explored exponential tails in Figure 2 for the 2D Gaussians with different L 's, Figure 3 for the 2D stretched exponential $\propto \exp(-|x|^{0.4})$ and Figure 4 for the heavy-tailed t-Student distribution with $\nu = 0.5$.

In the figures, the plots (a) exhibit the trajectory of particle at the labeled time step T with its velocity (green arrows). The color map indicates the speed of each particle: Blue (Low) \rightarrow Red (High), which is fixed for all figures. The contours indicate 25%, 50% percentile regions for the stretched exponential and 50%, 90% percentile regions for the Gaussian target distribution. The empirical Lipschitz-regularized f divergence (loss function) and the empirical Lipschitz-regularized Fisher Information are given in plots (b) and (c), respectively.



(a) (Top) $f = f_{\text{KL}}$ with $L = 1.0$, (Bottom) $f = f_{\text{KL}}$ with $L = 10.0$.



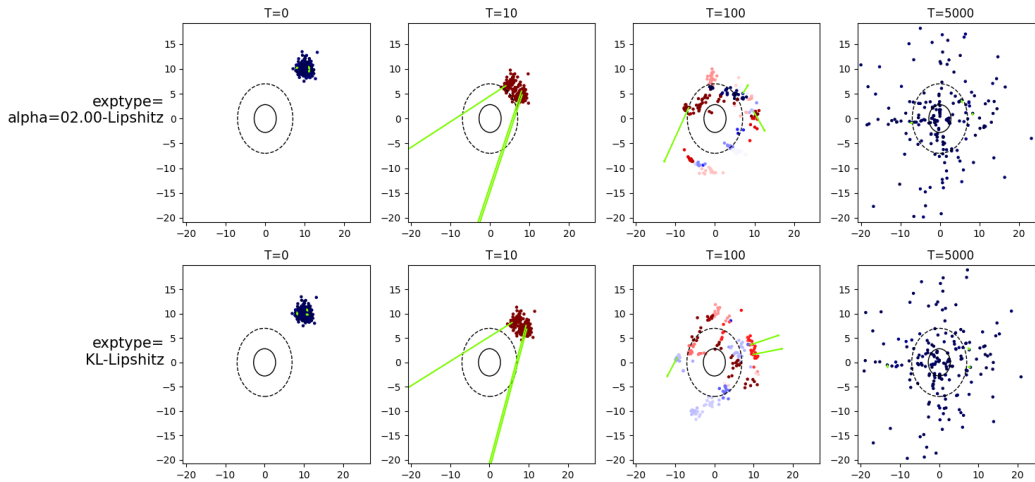
(b) KL-divergence

(c) Fisher information

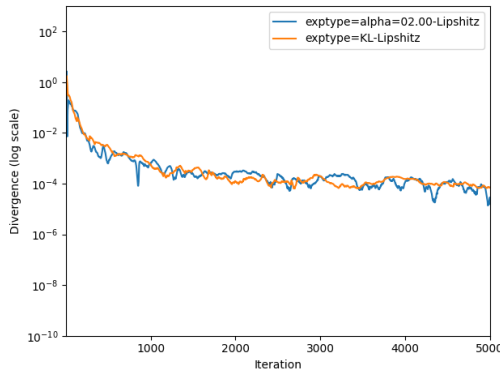
Figure 2: **(2D Gaussian Q , $\sigma_Q = 2$) The Lipschitz constraint L as a regularizer.** When learning Gaussians, particles can blow up without a regularization L . In fact, the size of L depends on data and affects the learning rate Δt . This observation is in alignment with the interpretation of L with the CFL condition in Section 6.2. In this example, $\sigma_Q = 2.0 > \sigma_P = 1.0$. For $L \geq 1$, we have convergence. However, $L = 100, \infty$ blew up within fixed learning rates $\gamma = 1.0, \delta = 0.05$ in Algorithm 1. $L = 100$ requires a careful choice of learning rates $\gamma = 10.0, \delta = 0.005$ to have a similar result. For most cases, $L = 1$ produces stable results.

7.2 HIGH DIMENSIONAL IMAGE DATA ON DIFFERENT TASKS

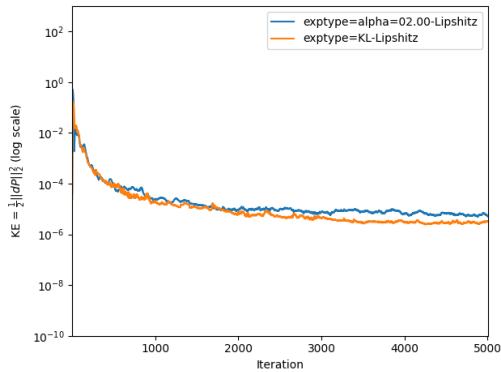
We compare the image generation performance of our $(f_{\text{KL}}, \Gamma_1)$ -GPA with $(f_{\text{KL}}, \Gamma_1)$ -GAN and Wasserstein GAN on MNIST, and in particular in a small target sample size regime. Precisely, we generate images of digits conditioning on their labels. See Figure 5 (a) - (f). CIFAR10 example in Appendix D.1 also testifies the ability of our algorithm to learn images without mode collapse in a small target sample size regime. In addition, we show from the image-to-image transformation example on MNIST, that the latent GPA improves the quality of the generated images as well as the computational efficiency. See Figure 5 (g) - (i) and Table 2. We note that latent GPA achieved the best FID score among the tested models. However, the success of the latent GPA is attained by the Q -perfect encoding auto-encoder. One more example working in a latent space shows the importance of Q -perfect encoding property for the latent GPA. See Appendix D.2.



(a) (Top) $f = f_\alpha$ with $\alpha = 2$ and $L = 1$, (Bottom) $f = f_{\text{KL}}$ with $L = 1$.



(b) Divergences



(c) Kinetic energy of particles

Figure 3: **(2D stretched exponential $\propto \exp(-|x|^{0.4})$, $\beta = 0.4$) The convergence in $f = f_{\text{KL}}$ and $f = f_\alpha$ with $\alpha = 2$.** This example has a heavier tail compared to the Gaussian ($\beta = 2 > 0.4$). (a) The trajectories of particles from KL flow given by (29) and $\alpha = 2$ flow given by (30) regularized by $L = 1$ look similar. The particles are transported to the 50 percentile region at an early stage and then redistributed. (b) For both f , the losses decrease without lots of fluctuations. The choice of $L = 1$ along with the learning rates $\gamma = 1.0$, $\delta = 0.05$ produces stable results. (c) The kinetic energies of the particle systems decay fast and converge. Indeed, the convergence of stretched exponentials is guaranteed by the classical functional inequalities of $f = \alpha$, KL gradient flows in Appendix A, B.

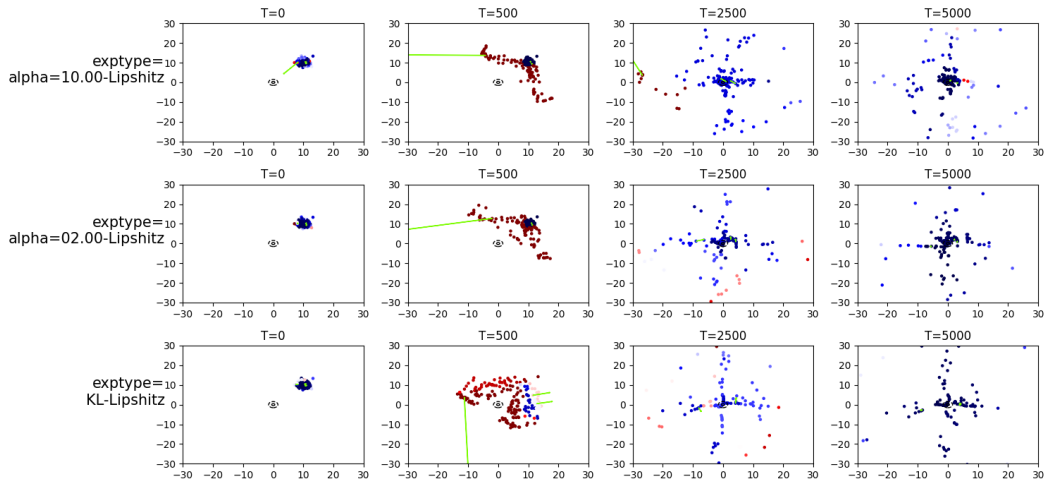
Conditioning on digit labels Figure 5	Sample size	200	2000
	$(f_{\text{KL}}, \Gamma_1)$ -GPA	4913.53	4926.91
	$(f_{\text{KL}}, \Gamma_1)$ -GAN	5603.55	1270.13
	Wasserstein-GAN	5653.20	1879.18
Digit transform Figure 6	\mathbb{R}^{64}	\mathbb{R}^{128}	$\mathbb{R}^{28 \times 28}$
	946.98	846.99	3710.23

(a) Final FID for MNIST data.

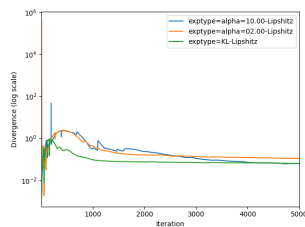
Space	Time
\mathbb{R}^{64}	949.408s
\mathbb{R}^{128}	999.862s
$\mathbb{R}^{28 \times 28}$	2549.594s

(b) Computation time for digit transform. Figure 6

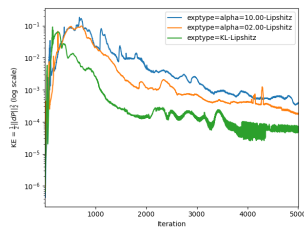
Table 2: MNIST performance summary.



(a) $L = 1$ (Top) $f = f_\alpha$ with $\alpha = 10$, (Middle) $f = f_\alpha$ with $\alpha = 2$, (Bottom) $f = f_{KL}$.



(b) Divergences



(c) Kinetic energy of particles

Figure 4: **(2D Student-t, $\nu = 0.5$) Convergence in selected choices of f :** 4 of 5 trials with f_{KL} ($\alpha = 1$) diverged, which implies the instability of the KL gradient flow. Instead, we use $f = f_\alpha$ with $\alpha = 10$ to handle the heavy tail. **green:** $f = f_{KL}$, **orange:** $f = f_\alpha$ with $\alpha = 2$, **blue:** $f = f_\alpha$ with $\alpha = 10$. (a) Transportation of particles and then redistribution. The contour indicates the 50% region. (b) The Lipschitz-regularized f_α divergence with $\alpha = 10$ converged in a lower value compared to the $\alpha = 2$ case. (c) The kinetic energy decays as divergence converges. Learning rates are chosen as $\gamma = 0.1, \delta = 0.01$. The f_{KL} plots correspond to the only converged simulation.

8 MERGING OF MICROARRAY GENE EXPRESSION DATA SETS

Our particle algorithms apart from generating new samples, they can transport any source distributions, including empirical ones, to an (empirical) target distribution. For instance, the image-to-image transformation example in the previous Section 7.2 and the batch effects removal example considered here. This is a distinguishing feature in relation to other generative flow models where the source needs to be of specific type (e.g. Gaussian), have an explicit and analytically-known probability density function or have suitable regularity properties (e.g., normalizing flows Chen et al. (2018a); Köhler et al. (2020); Chen et al. (2018b), diffusion models Sohl-Dickstein et al. (2015); Ho et al. (2020) or score-based generative flows Song & Ermon (2020); Song et al. (2021)). On the other hand, transforming samples from the source distribution to the target distribution might be handled using specialized GANs, e.g. CycleGAN Zhu et al. (2017) or StarGAN Choi et al. (2017). However, GANs require a large number of target samples while a small number of target samples (few hundreds) are enough for our GPA. Furthermore, combining our algorithm with representation learning, we can address the same problem on high dimensional data. These properties of our GPA are suitable for bioinformatics applications such as analysis of gene expression data. Gene expression datasets are not only high-dimensional but also small-sized thus it is crucial to increase the sample size by integrating together all available datasets from the same disease. However, this is not a straightforward process since it is well known that gene expression datasets may have different statistics even when they target the same disease; a phenomenon referred to as “batch effects” Tran et al. (2020). We propose to mitigate batch effects via the latent generative particle algorithm and match the statistics of

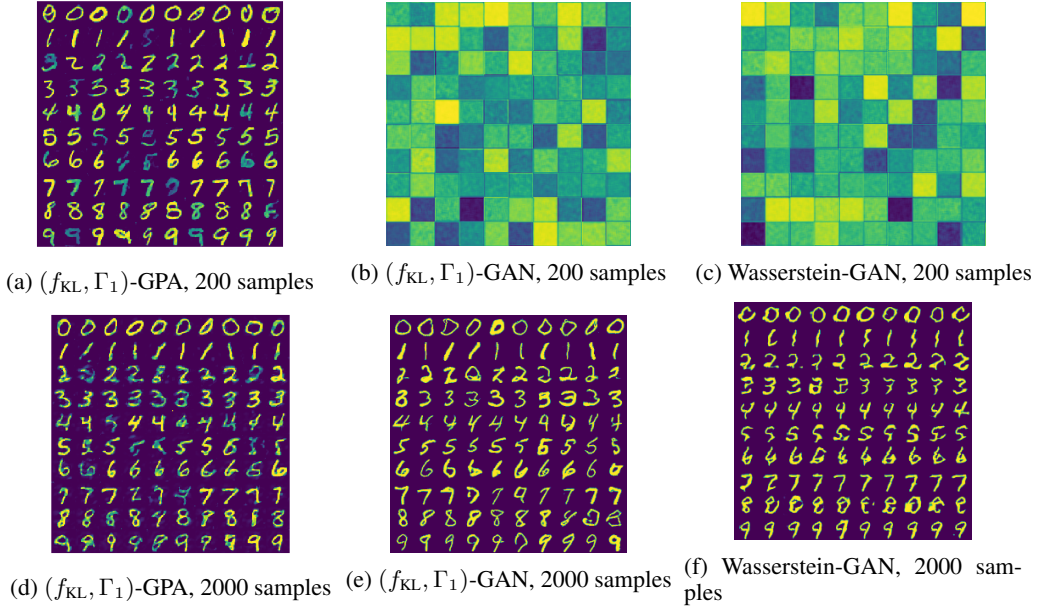


Figure 5: **MNIST; Learned digits by different generative models (column) with different number of training data (row).** The $(f_{\text{KL}}, \Gamma_1)$ -GPA was able to learn digits from a small data set, while the other methods failed. Using sufficiently large training data, GANs outperformed in capturing the scale, which can be observed by the more intense color contrast between a digit and its background. See FID scores in Table 2.

the two datasets. Figure 7 presents the results on applying our algorithm between two breast cancer datasets from the Gene Expression Omnibus (<https://www.ncbi.nlm.nih.gov/geo/>).

Dataset. We tested on publicly available gene expression data sets from Gene Expression Omnibus:

- Breast cancer: Accession number GSE47109 (206 samples), GSE10843 (245 samples)

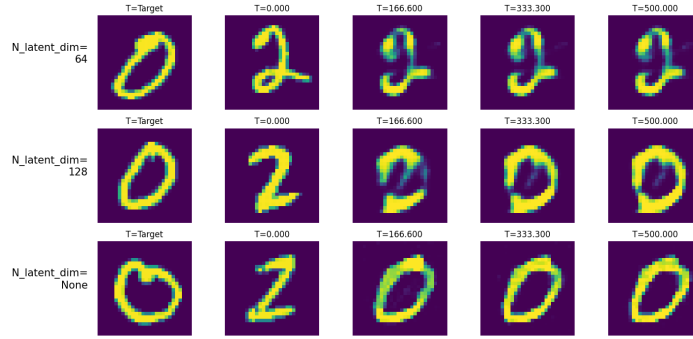
The former forms the source dataset, and the latter forms the target dataset. The source and the target data lie in the same dimensional space $\mathbb{R}^{54,675}$.

Auto-encoder. We applied PCA on the combined matrix for the source data and the target data which have been firstly normalized to mean zero and variance one. The normalized PCA can be interpreted as a linear auto-encoder. The PCA decoder is Lipschitz continuous with $L = \sqrt{d'}$. (Let $\mathbf{y} = \sum_{i=1}^{d'} z_i \mathbf{v}_i$, $\mathbf{y}' = \sum_{i=1}^{d'} z'_i \mathbf{v}_i \in \mathbb{R}^d$. The decoder $\mathcal{D}(\mathbf{z}) = \sum_{i=1}^{d'} z_i \mathbf{v}_i$ satisfies $\|\mathcal{D}(\mathbf{z}) - \mathcal{D}(\mathbf{z}')\| = \|\sum_{i=1}^{d'} (z_i - z'_i) \mathbf{v}_i\| \leq \|\mathbf{z} - \mathbf{z}'\| \sqrt{\sum_{i=1}^{d'} \|\mathbf{v}_i\|^2} = \sqrt{d'} \|\mathbf{z} - \mathbf{z}'\|$ by Cauchy-Schwarz inequality.)

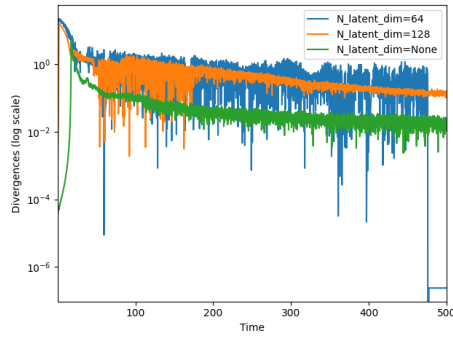
9 COMPARISON TO OTHER GENERATIVE MODELS

In this last Section, we discuss in some more detail the connections of our work to closely related methods such gradient flows in reproducing kernel Hilbert space (RKHS) spaces and generative flows such as normalizing flows, diffusion models, and score-based flows. We further demonstrate these connections and possible differences in the context of several computational examples.

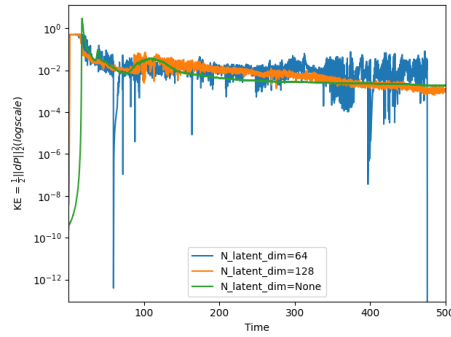
First, we note that the modeling approach in normalizing flows, diffusion models and score-based methods is to take small steps with explicit and thus trainable transition probabilities. In gradient flows, the transported distribution is always compared against the target distribution and not the probability density from the previous step. For this reason, in gradient flow particle methods, it is



(a) $(f_{\text{KL}}, \Gamma_1)$ -GPA. Transportations of particles in (Top) 64D, (Middle) 128D, (Bottom) 784D spaces



(b) $(f_{\text{KL}}, \Gamma_1)$ divergences



(c) Kinetic energy of particles

Figure 6: **MNIST digit transform $2 \rightarrow 0$; latent and original generative particles.** Latent particles are obtained by auto-encoders trained with 60,000 training images. Particles are transported in \mathbb{R}^{64} , \mathbb{R}^{128} , and $\mathbb{R}^{28 \times 28}$, respectively. (a) Time trajectories of particles in the real space. (b) $(f_{\text{KL}}, \Gamma_1)$ -divergence and (c) Kinetic energy of particles converged in 128D (orange) and 784D (green) spaces. 64D (blue) was unstable. See FID scores and computation time in Table 2.

necessary to deploy divergences or metrics between probability distributions which can be mutually singular, such as between empirical distributions of generative particles and target data. Indeed, the MMD gradient flow Arbel et al. (2019) utilizes an integral probability metrics (IPMs) where the witness function is constructed as a minimizer in an RKHS unit ball. Despite its ability to handle mutually singular distributions, MMD lacks convexity due to the use of an IPM. Therefore the MMD gradient flow itself does not guarantee the convergence to a target, as is also observed in experiments, see for instance Arbel et al. (2019) and Section 9 of this paper. By contrast, our particle gradient flows rely on (f, Γ) divergences which have strong convexity properties as pointed out in Birrell et al. (2022a). We note here that another critical difference between our approach and RKHS-based gradient flows is that the latter methods carry out divergence or IPM estimation over a linear space (such as an RKHS) rather than over much richer spaces of neural networks. For this reason RKHS-based MMD and KALE gradient flows Arbel et al. (2019); Glaser et al. (2021) seem to be practically confined to systems of lower dimension; in contrast, our methods which are neural network-based, perform well for high-dimensional data sets such as MNIST and CIFAR-10. Computational comparisons between our particle methods and RKHS-based particle methods are discussed in the examples later in this Section.

As noted in the Introduction, normalizing flows, diffusion models and score-based methods are likelihood-based, while gradient flows depend on more flexible choices of divergences or IPMs, much like GANs. Next we discuss some further connections and differences between these methods and the proposed Lipschitz-regularized particle gradient flows. Our particle algorithms can not only generate new samples, but importantly they can transport any source distributions, including empirical ones, to an empirical target distribution, such as in the gene expression data integration examples in Section 8. This feature is due to the (f, Γ) -divergences which remain finite even for non-absolutely continuous distributions, and are used here to define the gradient flow in probability

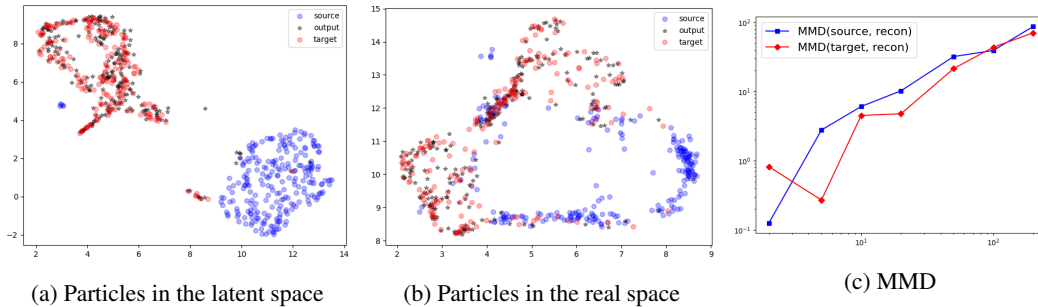


Figure 7: **(Gene expression data; Merging Breast Cancer datasets)**. We merged gene data using our latent GPA in significantly lower dimensions. Two distinct gene data sets but from the same disease decrease their dimension from 54,675D into $d' = 2, 5, 10, 20, 50, 100, 200$ using normalized PCA. Then, latent particles are transported using GPA. **blue: source, red: target, black: transported.** (a) Latent particles in the $\mathbb{R}^{d'}$ with $d' = 20$ which are encoded by the PCA. (b) Transported samples are reconstructed to the real space. The 2D visualizations are obtained using the UMAP algorithm McInnes et al. (2018). (c) The MMD distance Gretton et al. (2012) between the reconstructed datasets: **blue: $\text{MMD}(P_0^{\mathcal{Y}}, P_T^{\mathcal{Y}})$, red: $\text{MMD}(Q^{\mathcal{Y}}, P_T^{\mathcal{Y}})$** , $T = 25K$. The transported distribution has smaller distances from the target distribution when $d' = 5, 10, 20, 50, 200$.

space. This capability is also a distinguishing aspect of our methods with respect to other generative flow models such as normalizing flows Chen et al. (2018a); Köhler et al. (2020); Chen et al. (2018b), diffusion models Sohl-Dickstein et al. (2015); Ho et al. (2020) or score-based generative flows Song & Ermon (2020); Song et al. (2021), where the source may need to have a simple and analytically-known probability density function with sufficient regularity properties for likelihood and score-related calculations. For instance, score-based methods require some regularity assumptions between generated and target distributions: first, since they solve a Fokker Planck equation (FPE), they are equivalent to a KL gradient flow in probability space; and thus implicitly require the absolute continuity of the solution of the FPE with respect to the target. Therefore, adding noise is typically necessary in score-based methods due to a lack of sufficient data, manifested theoretically as a breakdown of absolute continuity between source and target. Second, score-based methods require that the source distribution and eventually the data distribution produced as solutions to the FPE are sufficiently regular. Regarding both points we note that our gene expression data integration example in Section 8 is exactly not in that regularity category since source and target are only available as (singular) empirical distributions with low sample size. We also include a computational comparison between score-based methods and Lipschitz-regularized gradient particle flows at the end of the Section in the context of a two-dimensional Gaussian mixture model.

2D Mixture of Gaussians. The target distribution Q consists of 4 wells of 2D Gaussian distributions with the same standard deviation 0.5 and centered at $(0, 0), (4, 0), (0, 4), (4, 4)$, respectively. We transport 200 samples from an initial Gaussian distribution P centered on the well at $(4, 4)$ and with standard deviation 0.5.

We compare the performance of $(f_{\text{KL}}, \Gamma_L)$ -generative particle algorithm with the corresponding GAN, as well as gradient flows such as KALE flow Glaser et al. (2021) and MMD flow Arbel et al. (2019), and the KL unadjusted Langevin algorithm Durmus & Éric Moulines (2017). We can compare the behaviors of our generative particle algorithm and GAN, and its dependence on the Lipschitz regularization L . The $(f_{\text{KL}}, \Gamma_L)$ -generative particle algorithm and KALE flow use different regularization techniques where the former provides an interpolation between KL divergence and Wasserstein metric (Γ_1) and the latter provides an interpolation between KL divergence and Maximum Mean Discrepancy (MMD). We observed that the former captured the four wells while the latter failed. The comparison with KL ULA and MMD flow suggests that the use of regularization enables the convergence without further techniques such as adding noise. See Figure 8.

2D Mixture of Gaussians embedded in 12D. The target distribution Q is a mixture of 2D Gaussians (as in the previous example) but supported in a plane embedded in 12 dimensional space. In

Figure 9 we compare the performance of $(f_{\text{KL}}, \Gamma_1)$ -generative particle algorithm with the corresponding GAN and Wasserstein GAN, in the sense of transportation and redistribution of the mass in the plane supporting the distribution and its orthogonal subspace. $L = 1$ is fixed. A Gaussian distribution centered at $(5, \dots, 5) \in \mathbb{R}^{12}$ and with standard deviation 0.5 is picked as the initial distribution P for the $(f_{\text{KL}}, \Gamma_1)$ -generative particle algorithm.

2D Mixture of two Gaussians. The target distribution Q is a mixture of two 2D Gaussians $0.8 * N((5, 5), I_2) + 0.2 * N((-5, -5), I_2)$ which is presented in Song & Ermon (2020). The two Gaussian wells are sufficiently far away (taking also into account their covariances) and have different weights. The authors in Song & Ermon (2020) demonstrated that a simple score matching algorithm might not estimate the score for Q accurately in low probability regions and it does not reflect the weights on mixing two distributions in case that the initial samples are chosen uniformly in the entire region $[-8, 8] \times [-8, 8]$. Song & Ermon (2020) suggests that putting different (decreasing) noises when propagating particles through Langevin dynamics (i.e. using annealed Langevin dynamics) alleviates the problem. We modify the example by sampling initial data from one well $N((5, 5), I_2)$ and compare the samples after 10K steps of our method and score matching with (annealed) Langevin dynamics. We demonstrate with this example that transportation of particles from KL Lipschitz regularized flow can capture the other well without tuning a noise term (just deterministic particles are sufficient), as well as capture the mixing ratio of two distributions. See Figure 10.

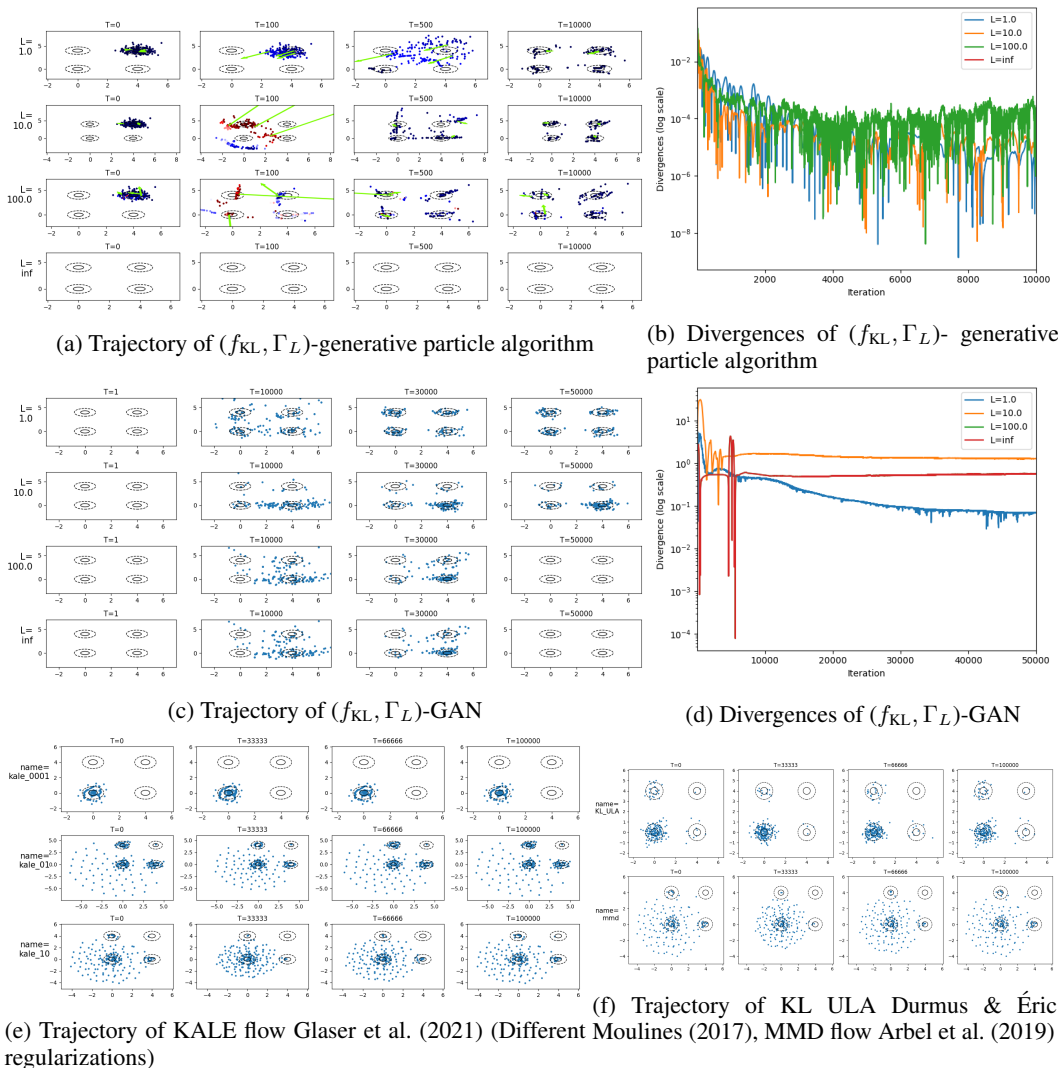


Figure 8: (2D Mixture of Gaussians) Comparison between different methods. (a) $(f_{\text{KL}}, \Gamma_L)$ -generative particles algorithm with different values for L . The particles are transported to the 4 wells faster as L gets larger, however for large L the algorithm become unstable ($L \geq 100$). Learning rates are chosen as $\gamma = 1.0, \delta = 0.005$. (c) Comparison with $(f_{\text{KL}}, \Gamma_L)$ -GAN which has the same discriminator as $(f_{\text{KL}}, \Gamma_L)$ -generative particles algorithm but a different generator mechanism. $(f_{\text{KL}}, \Gamma_L)$ -generative particles algorithm converges 3-5 times faster compared to $(f_{\text{KL}}, \Gamma_L)$ -GAN. The time step for second column of (c) corresponds to the last column of (a). (b)+(d) The values of the loss function for $(f_{\text{KL}}, \Gamma_L)$ -GAN are less oscillatory when compared to $(f_{\text{KL}}, \Gamma_L)$ -generative particles algorithm, however their corresponding divergence is at least one order of magnitude larger than the $(f_{\text{KL}}, \Gamma_L)$ -generative particles algorithm. (e) KALE flow can be compared with $(f_{\text{KL}}, \Gamma_L)$ -generative particles algorithm in the sense of being a different regularization technique. The KALE gradient flow regularizes the RKHS norm of ϕ^* while $(f_{\text{KL}}, \Gamma_L)$ -generative particles algorithm regularizes the norm of $\nabla \phi^*$. The KALE flow Glaser et al. (2021) fails to capture the 4 wells in a reasonable amount of time. Here a Gaussian kernel with $\sigma = 0.5$ is chosen for the RKHS kernel. Learning rate is chosen as 0.001. (f) Bottom: MMD Arbel et al. (2019) gradient flow (without extra noise). A Gaussian kernel with $\sigma = 0.5$ is used for the RKHS. Top: For comparison KL gradient flow trained with the unadjusted Langevin algorithm (ULA) Durmus & Éric Moulines (2017). Learning rate is chosen as 0.001.

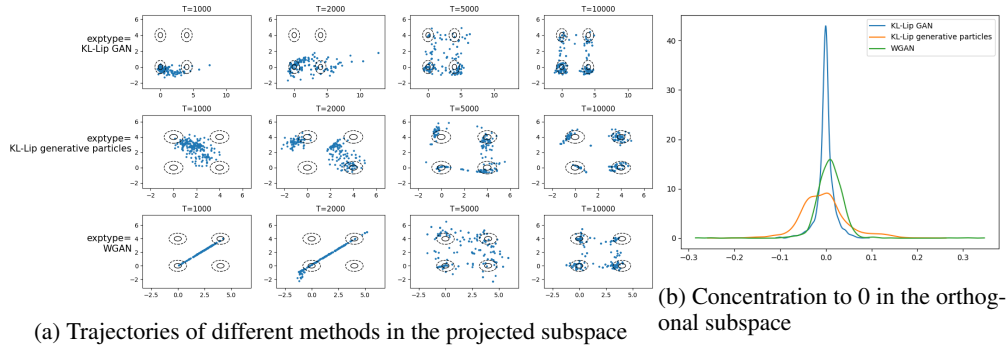


Figure 9: **(2D Mixture of Gaussians embedded in 12D, 5000 target samples) Comparison between different methods.** (a) The time trajectories in the 2D projected subspace of $(f_{\text{KL}}, \Gamma_1)$ -GAN (top), $(f_{\text{KL}}, \Gamma_1)$ -generative particles algorithm (center), Wasserstein-GAN (bottom). (b) Particle distributions, projected onto components orthogonal to the support plane. Values concentrated around 0 indicate convergence to the sub-manifold supporting the distribution. 5000 target samples are used with mini-batch scheme with $N_{\text{mb}} = 200$. $L = 1$ is fixed. Learning rates are chosen as $\gamma = 0.25, \delta = 0.005$ for the $(f_{\text{KL}}, \Gamma_1)$ -generative particles algorithm.

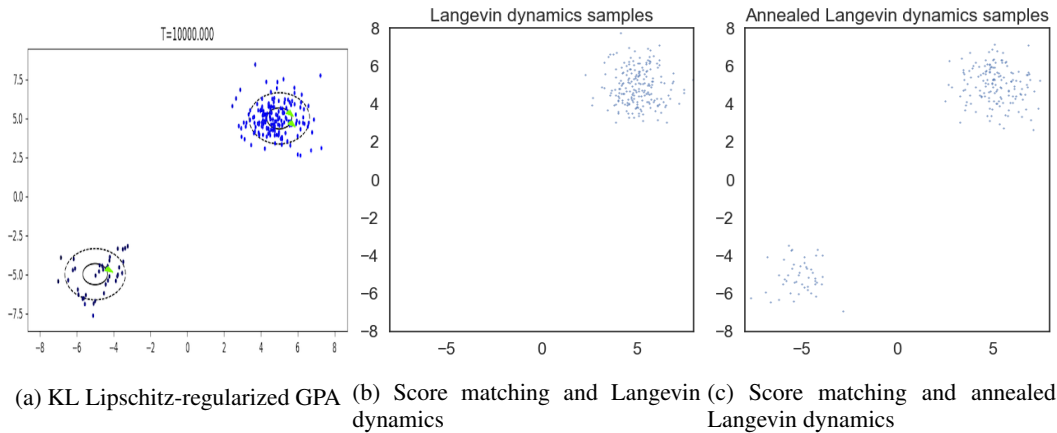


Figure 10: **(2D Mixture of two Gaussians) Comparison with score based model.** 200 initial samples (particles) are chosen from the one well $N((5, 5), I_2)$. The target distribution is the mixture of two Gaussians $0.8 * N((5, 5), I_2) + 0.2 * N((-5, -5), I_2)$. 200 samples are chosen from the target distribution Q . (a) KL Lipschitz regularized GPA captures the other well in a disjoint support as well as capture the mixing ratio (0.8, 0.19) of two distributions. (b) Score-based generative Langevin dynamics fails to find the other well; as also expected from the previous ULA example with a known form of Q in Figure 8(f). (c) However, annealed score-based dynamics Song & Ermon (2020); Song et al. (2021) can discover the other well and the different mixing ratio (0.76, 0.235) for the two Gaussian distributions.

Acknowledgement: The research of P.B., H.G., M.K., Y.P. and L.R.-B. was partially supported by the Air Force Office of Scientific Research (AFOSR) under the grant FA9550-21-1-0354. The research of M. K. and L.R.-B. was partially supported by the National Science Foundation (NSF) under the grants DMS-2008970 and TRIPODS CISE-1934846. The research of P. B. and H. G. was partially supported by the National Science Foundation (NSF) under the grant DMS-2008970. The work of Y.P. was partially supported by the Hellenic Foundation for Research and Innovation (HFRI) through the “Second Call for HFRI Research Projects to support Faculty Members and Researchers” under Project 4753.

REFERENCES

- Luigi Ambrosio, Nicola Gigli, and Giuseppe Savaré. *Gradient flows: in metric spaces and in the space of probability measures*. Springer Science & Business Media, 2005.
- Michael Arbel, Anna Korba, Adil SALIM, and Arthur Gretton. Maximum mean discrepancy gradient flow. In H. Wallach, H. Larochelle, A. Beygelzimer, F. d'Alché-Buc, E. Fox, and R. Garnett (eds.), *Advances in Neural Information Processing Systems*, volume 32. Curran Associates, Inc., 2019. URL <https://proceedings.neurips.cc/paper/2019/file/944a5ae3483ed5c1e10bbccb7942a279-Paper.pdf>.
- Martin Arjovsky, Soumith Chintala, and Léon Bottou. Wasserstein generative adversarial networks. In Doina Precup and Yee Whye Teh (eds.), *Proceedings of the 34th International Conference on Machine Learning*, volume 70 of *Proceedings of Machine Learning Research*, pp. 214–223. PMLR, 06–11 Aug 2017. URL <https://proceedings.mlr.press/v70/arjovsky17a.html>.
- Jeremiah Birrell, Paul Dupuis, Markos A Katsoulakis, Yannis Pantazis, and Luc Rey-Bellet. (f, gamma)-divergences: Interpolating between f-divergences and integral probability metrics. *Journal of Machine Learning Research*, 23(39):1–70, 2022a.
- Jeremiah Birrell, Markos A. Katsoulakis, and Yannis Pantazis. Optimizing variational representations of divergences and accelerating their statistical estimation. *IEEE Transactions on Information Theory*, pp. 1–1, 2022b. doi: 10.1109/TIT.2022.3160659.
- Jeremiah Birrell, Markos A. Katsoulakis, Luc Rey-Bellet, and Wei Zhu. Structure-preserving gans. In Kamalika Chaudhuri, Stefanie Jegelka, Le Song, Csaba Szepesvári, Gang Niu, and Sivan Sabato (eds.), *International Conference on Machine Learning, ICML 2022, 17-23 July 2022, Baltimore, Maryland, USA*, volume 162 of *Proceedings of Machine Learning Research*, pp. 1982–2020. PMLR, 2022c. URL <https://proceedings.mlr.press/v162/birrell122a.html>.
- Nicholas M. Boffi and Eric Vanden-Eijnden. Probability flow solution of the Fokker-Planck equation. *arXiv e-prints*, art. arXiv:2206.04642, June 2022.
- John W. Cahn. Phase separation by spinodal decomposition in isotropic systems. *The Journal of Chemical Physics*, 42(1):93–99, 1965. doi: 10.1063/1.1695731. URL <https://doi.org/10.1063/1.1695731>.
- José Carrillo, Jean Dolbeault, Ivan Gentil, and Ansgar Juengel. Entropy-energy inequalities and improved convergence rates for nonlinear parabolic equations. *Discrete and Continuous Dynamical Systems-Series B*, 6(5):1027–1050, 2006.
- José Antonio Carrillo, Yanghong Huang, Francesco Saverio Patacchini, and Gershon Wolansky. Numerical study of a particle method for gradient flows. *Kinetic and Related Models*, 10(3): 613–641, 2017.
- Changyou Chen, Chunyuan Li, Liqun Chen, Wenlin Wang, Yunchen Pu, and Lawrence Carin Duke. Continuous-time flows for efficient inference and density estimation. In Jennifer Dy and Andreas Krause (eds.), *Proceedings of the 35th International Conference on Machine Learning*, volume 80 of *Proceedings of Machine Learning Research*, pp. 824–833. PMLR, 10–15 Jul 2018a. URL <https://proceedings.mlr.press/v80/chen18d.html>.
- Ricky T. Q. Chen, Yulia Rubanova, Jesse Bettencourt, and David K Duvenaud. Neural ordinary differential equations. In S. Bengio, H. Wallach, H. Larochelle, K. Grauman, N. Cesa-Bianchi, and R. Garnett (eds.), *Advances in Neural Information Processing Systems*, volume 31. Curran Associates, Inc., 2018b. URL <https://proceedings.neurips.cc/paper/2018/file/69386f6bb1dfed68692a24c8686939b9-Paper.pdf>.
- Yunjey Choi, Min-Je Choi, Munyoung Kim, Jung-Woo Ha, Sunghun Kim, and Jaegul Choo. Stargan: Unified generative adversarial networks for multi-domain image-to-image translation. *CoRR*, abs/1711.09020, 2017. URL <http://dblp.uni-trier.de/db/journals/corr/corr1711.html#abs-1711-09020>.

-
- Jean Dolbeault, Ivan Gentil, Arnaud Guillin, and Feng-Yu Wang. L^q -functional inequalities and weighted porous media equations. *Potential Anal.*, 28(1):35–59, 2008. ISSN 0926-2601. doi: 10.1007/s11118-007-9066-0. URL <https://doi.org/10.1007/s11118-007-9066-0>.
- Paul Dupuis and Yixiang Mao. Formulation and properties of a divergence used to compare probability measures without absolute continuity. *ESAIM Control Optim. Calc. Var.*, 28:Paper No. 10, 38, 2022. ISSN 1292-8119. doi: 10.1051/cocv/2022002. URL <https://doi.org/10.1051/cocv/2022002>.
- Alain Durmus and Éric Moulines. Nonasymptotic convergence analysis for the unadjusted Langevin algorithm. *The Annals of Applied Probability*, 27(3):1551 – 1587, 2017. doi: 10.1214/16-AAP1238. URL <https://doi.org/10.1214/16-AAP1238>.
- Aude Genevay, Marco Cuturi, Gabriel Peyré, and Francis Bach. Stochastic optimization for large-scale optimal transport. In D. Lee, M. Sugiyama, U. Luxburg, I. Guyon, and R. Garnett (eds.), *Advances in Neural Information Processing Systems*, volume 29. Curran Associates, Inc., 2016. URL <https://proceedings.neurips.cc/paper/2016/file/2a27b8144ac02f67687f76782a3b5d8f-Paper.pdf>.
- Pierre Glaser, Michael Arbel, and Arthur Gretton. Kale flow: A relaxed kl gradient flow for probabilities with disjoint support. In M. Ranzato, A. Beygelzimer, Y. Dauphin, P.S. Liang, and J. Wortman Vaughan (eds.), *Advances in Neural Information Processing Systems*, volume 34, pp. 8018–8031. Curran Associates, Inc., 2021. URL <https://proceedings.neurips.cc/paper/2021/file/433a6ea5429d6d75f0be9bf9da26e24c-Paper.pdf>.
- Ian Goodfellow, Jean Pouget-Abadie, Mehdi Mirza, Bing Xu, David Warde-Farley, Sherjil Ozair, Aaron Courville, and Yoshua Bengio. Generative adversarial nets. *Advances in neural information processing systems*, 27, 2014.
- Arthur Gretton, Karsten M. Borgwardt, Malte J. Rasch, Bernhard Schölkopf, and Alexander Smola. A kernel two-sample test. *J. Mach. Learn. Res.*, 13:723–773, March 2012. ISSN 1532-4435. URL <http://dl.acm.org/citation.cfm?id=2188385.2188410>.
- Ishaan Gulrajani, Faruk Ahmed, Martin Arjovsky, Vincent Dumoulin, and Aaron C Courville. Improved training of wasserstein gans. In I. Guyon, U. Von Luxburg, S. Bengio, H. Wallach, R. Fergus, S. Vishwanathan, and R. Garnett (eds.), *Advances in Neural Information Processing Systems*, volume 30. Curran Associates, Inc., 2017. URL <https://proceedings.neurips.cc/paper/2017/file/892c3b1c6dcd52936e27cbd0ff683d6-Paper.pdf>.
- Jonathan Ho, Ajay Jain, and Pieter Abbeel. Denoising diffusion probabilistic models, 2020.
- Jacob J Hughey and Atul J Butte. Robust meta-analysis of gene expression using the elastic net. *Nucleic acids research*, pp. gkv229, 2015.
- Diederik P Kingma and Max Welling. Auto-Encoding Variational Bayes. *arXiv e-prints*, art. arXiv:1312.6114, December 2013.
- Jonas Köhler, Leon Klein, and Frank Noe. Equivariant flows: Exact likelihood generative learning for symmetric densities. In Hal Daumé III and Aarti Singh (eds.), *Proceedings of the 37th International Conference on Machine Learning*, volume 119 of *Proceedings of Machine Learning Research*, pp. 5361–5370. PMLR, 13–18 Jul 2020. URL <https://proceedings.mlr.press/v119/kohler20a.html>.
- Yann LeCun, Sumit Chopra, Raia Hadsell, Marc’Aurelio Ranzato, and Fu-Jie Huang. A tutorial on energy-based learning. In G. Bakir, T. Hofman, B. Schölkopf, A. Smola, and B. Taskar (eds.), *Predicting Structured Data*. MIT Press, 2006.
- Randall LeVeque. *Finite Difference Methods for Ordinary and Partial Differential Equations: Steady-State and Time-Dependent Problems (Classics in Applied Mathematics Classics in Applied Mathemat)*. Society for Industrial and Applied Mathematics, USA, 2007. ISBN 0898716292.

-
- Qiang Liu. Stein variational gradient descent as gradient flow. In I. Guyon, U. Von Luxburg, S. Bengio, H. Wallach, R. Fergus, S. Vishwanathan, and R. Garnett (eds.), *Advances in Neural Information Processing Systems*, volume 30. Curran Associates, Inc., 2017. URL <https://proceedings.neurips.cc/paper/2017/file/17ed8abedc255908be746d245e50263a-Paper.pdf>.
- Qiang Liu and Dilin Wang. Stein variational gradient descent: A general purpose bayesian inference algorithm. In D. Lee, M. Sugiyama, U. Luxburg, I. Guyon, and R. Garnett (eds.), *Advances in Neural Information Processing Systems*, volume 29. Curran Associates, Inc., 2016. URL <https://proceedings.neurips.cc/paper/2016/file/b3ba8f1bee1238a2f37603d90b58898d-Paper.pdf>.
- Jianfeng Lu, Yulong Lu, and James Nolen. Scaling limit of the stein variational gradient descent: The mean field regime. *SIAM Journal on Mathematical Analysis*, 51(2):648–671, 2019. doi: 10.1137/18M1187611. URL <https://doi.org/10.1137/18M1187611>.
- Dimitra Maoutsa, Sebastian Reich, and Manfred Opper. Interacting particle solutions of fokker–planck equations through gradient–log–density estimation. *Entropy*, 22(8), 2020. ISSN 1099-4300. doi: 10.3390/e22080802. URL <https://www.mdpi.com/1099-4300/22/8/802>.
- Peter A Markowich and Cédric Villani. On the trend to equilibrium for the fokker-planck equation: an interplay between physics and functional analysis. *Mat. Contemp.*, 19:1–29, 2000.
- Leland McInnes, John Healy, Nathaniel Saul, and Lukas Großberger. Umap: Uniform manifold approximation and projection. *Journal of Open Source Software*, 3(29):861, 2018. doi: 10.21105/joss.00861. URL <https://doi.org/10.21105/joss.00861>.
- Takeru Miyato, Toshiki Kataoka, Masanori Koyama, and Yuichi Yoshida. Spectral normalization for generative adversarial networks. 02 2018.
- Youssef Mroueh, Tom Sercu, and Anant Raj. Sobolev descent. In *The 22nd International Conference on Artificial Intelligence and Statistics*, pp. 2976–2985. PMLR, 2019.
- F. Otto and C. Villani. Generalization of an inequality by talagrand and links with the logarithmic sobolev inequality. *Journal of Functional Analysis*, 173(2):361–400, 2000. ISSN 0022-1236. doi: <https://doi.org/10.1006/jfan.1999.3557>. URL <https://www.sciencedirect.com/science/article/pii/S0022123699935577>.
- Felix Otto. The geometry of dissipative evolution equations: the porous medium equation. *Comm. Partial Differential Equations*, 26(1-2):101–174, 2001. ISSN 0360-5302. doi: 10.1081/PDE-100002243. URL <https://doi.org/10.1081/PDE-100002243>.
- Sebastian Reich and Simon Weissmann. Fokker–planck particle systems for bayesian inference: Computational approaches. *SIAM/ASA Journal on Uncertainty Quantification*, 9(2):446–482, 2021. doi: 10.1137/19M1303162. URL <https://doi.org/10.1137/19M1303162>.
- Gareth O. Roberts and Richard L. Tweedie. Exponential convergence of Langevin distributions and their discrete approximations. *Bernoulli*, 2(4):341 – 363, 1996. doi: [bj/1178291835](https://doi.org/10.1080/10236199608839531). URL <https://doi.org/10.1080/10236199608839531>.
- Robin Rombach, Andreas Blattmann, Dominik Lorenz, Patrick Esser, and Björn Ommer. High-resolution image synthesis with latent diffusion models. *CoRR*, abs/2112.10752, 2021. URL <https://arxiv.org/abs/2112.10752>.
- Jascha Sohl-Dickstein, Eric A. Weiss, Niru Maheswaranathan, and Surya Ganguli. Deep unsupervised learning using nonequilibrium thermodynamics, 2015.
- Yang Song and Stefano Ermon. Generative modeling by estimating gradients of the data distribution, 2020.
- Yang Song, Jascha Narain Sohl-Dickstein, Diederik P. Kingma, Abhishek Kumar, Stefano Ermon, and Ben Poole. Score-based generative modeling through stochastic differential equations. *ArXiv*, abs/2011.13456, 2021.

-
- Marc Stieffenhofer, Tristan Bereau, and Michael Wand. Adversarial reverse mapping of condensed-phase molecular structures: Chemical transferability. *APL Materials*, 9:031107, 03 2021. doi: 10.1063/5.0039102.
- Jonatan Taminau, Cosmin Lazar, Stijn Meganck, and Ann Nowé. Comparison of merging and meta-analysis as alternative approaches for integrative gene expression analysis. *ISRN bioinformatics*, 2014, 2014.
- Guiseppe Toscani and Cédric Villani. On the trend to equilibrium for some dissipative systems with slowly increasing a priori bounds. *Journal of Statistical Physics*, 98(5):1279–1309, 2000.
- Hoa Thi Nhu Tran, Kok Siong Ang, Marion Chevrier, Xiaomeng Zhang, Nicole Yee Shin Lee, Michelle Goh, and Jinmiao Chen. A benchmark of batch-effect correction methods for single-cell rna sequencing data. *Genome Biology*, 21(1):12–12, 2020. ISSN 1474-760X.
- Juan Luis Vázquez. Barenblatt solutions and asymptotic behaviour for a nonlinear fractional heat equation of porous medium type. *Journal of the European Mathematical Society*, 16(4):769–803, 2014.
- Pantelis Vlachas, Georgios Arampatzis, Caroline Uhler, and Petros Koumoutsakos. Multiscale simulations of complex systems by learning their effective dynamics. *Nature Machine Intelligence*, 03 2022. doi: 10.48550/arXiv.2006.13431.
- Feng-Yu Wang. A generalization of Poincaré and log-Sobolev inequalities. *Potential Anal.*, 22(1): 1–15, 2005. ISSN 0926-2601. doi: 10.1007/s11118-004-4006-8. URL <https://doi.org/10.1007/s11118-004-4006-8>.
- Feng-Yu Wang. Orlicz–poincaré inequalities. *Proceedings of the Edinburgh Mathematical Society*, 51(2):529–543, 2008.
- Qiao Wang, Geng Zhang, Yajie Li, Zijian Hong, Da Wang, and Siqi Shi. Application of phase-field method in rechargeable batteries. *npj Computational Materials*, 6(1):1–8, 2020.
- Wujie Wang and Rafael Gómez-Bombarelli. Coarse-graining auto-encoders for molecular dynamics. *npj Computational Materials*, 5:125, 12 2019. doi: 10.1038/s41524-019-0261-5.
- Jingzhi Zhu, Long-Qing Chen, Jie Shen, and Veena Tikare. Coarsening kinetics from a variable-mobility cahn-hilliard equation: Application of a semi-implicit fourier spectral method. *Physical Review E*, 60(4):3564, 1999.
- Jun-Yan Zhu, Taesung Park, Phillip Isola, and Alexei A Efros. Unpaired image-to-image translation using cycle-consistent adversarial networks. In *Computer Vision (ICCV), 2017 IEEE International Conference on*, 2017.

A FOKKER-PLANCK EQUATION, AND ITS CONVERGENCE TO EQUILIBRIUM STATE

Generalized Fokker Planck as the gradient flow of f -divergences. Let p_t is the density of P_t . The associated gradient flow is given by the generalized Fokker-Planck equation

$$\partial_t p_t = \nabla \cdot \left(p_t \nabla \frac{\delta D_f(P\|Q)}{\delta P}(p_t) \right) = \nabla \cdot \left(p_t \nabla f' \left(\frac{p_t}{q} \right) \right) \quad (33)$$

The Fokker Planck as gradient flow of KL. When $f = f_{\text{KL}}$, we obtain the known Fokker-Planck equation

$$\partial_t p_t - \Delta p_t + \nabla \cdot \left(p_t \frac{\nabla q}{q} \right) = 0.$$

A.1 EXPONENTIAL DECAY WHEN $q \propto e^{-V}$ AND V IS λ -CONVEX

In this section for simplicity that the probability densities of both source and target distributions exist and are denoted by p, q . We consider the Cauchy problem of the Fokker-Planck equation given in Section 6 with

$$p(t = 0, \cdot) = p \geq 0 \text{ and } \int p = 1. \quad (34)$$

The next theorem in Markowich & Villani (2000) gives us the conditions that a probability measure satisfies in order to logarithmic Sobolev inequalities and consequently exponential decay.

Theorem A.1. *Let $q \in L^1(\mathbb{R}^d)$ and V be λ -convex (i.e. $D^2V(x) \geq \lambda I_d$ for all $x \in \mathbb{R}^d$), where I_d is the identity matrix of dimension d . Then, q satisfies a logarithmic Sobolev inequality with constant λ , i.e. $D_{\text{KL}}(p\|q) \leq \frac{1}{2\lambda} I(p\|q)$, and the solution of the homogeneous Fokker-Planck equation goes to equilibrium in KL divergence, with a rate $e^{-2\lambda t}$ at least.*

Typical examples that satisfy the conditions of Theorem A.1 are

$$q(x) = \frac{e^{-|x|^\beta}}{\int e^{-|x|^\beta}}, \text{ for } x \in \mathbb{R}^d \quad \text{with} \quad \beta \geq 2 \quad (35)$$

When $\beta = 2$, the target probability distribution with density q is the Gaussian with variance σ and zero mean, i.e.

$$q(x) = \frac{1}{(2\pi\sigma)^{d/2}} e^{-\frac{|x|^2}{2\sigma}},$$

(i.e. $V(x) = \frac{|x|^2}{2\sigma}$). By applying Theorem A.1, we get that for any initial probability distribution P which is absolutely continuous with respect to Q ,

$$D_{\text{KL}}(p_t\|q) \leq D_{\text{KL}}(p_0\|q) e^{-2t/\sigma} \quad (36)$$

where we have also used that the Stam-Gross Logarithmic Sobolev inequality, i.e. $D_{\text{KL}}(p\|q) \leq \frac{\sigma}{2} I(p\|q)$, see formula (14) in Markowich & Villani (2000).

A.2 POLYNOMIAL DECAY WHEN $q \propto e^{-V}$ AND V IS DEGENERATELY CONVEX AT INFINITY

We consider a potential $V \in W_{\text{loc}}^{2,\infty}$ such that $\int q = 1$ and degenerately convex at infinity, i.e.

$$U(u) - a \leq V(u) \leq U(u) + b \quad (37)$$

where a, b are nonnegative constants and U is convex degenerate, i.e.

$$D^2U(u) \geq c(1 + |u|)^{\beta-2}, \quad c > 0 \text{ and } \beta \in (0, 2) \quad (38)$$

Without loss of generality we assume that U takes its unique minimum at 0. We further assume that for some $b, c, C_0 > 0$

$$\nabla V(u) \cdot u \geq c|u|^b - C_0 \quad (39)$$

A typical potential that satisfies equation 37, equation 38 and equation 39 is $V = |x|^\beta$ with $0 < \beta < 2$. Before we state the next theorem in Toscani & Villani (2000), we further define the following quantities

$$M_s(p) := \int p(x)(1 + |x|^2)^{s/2}, \quad s > 2 \text{ and } \delta := \frac{2 - \beta}{2(2 - \beta) + (s - 2)} \in (0, \frac{1}{2}) \quad (40)$$

Theorem A.2. *Let V be a potential satisfying assumptions equation 37, equation 38 and equation 39. Let p_0 be a probability density such that $D_{\text{KL}}(p_0\|q) < \infty$, $M_s(p_0) < \infty$ given in equation 40 for $s > 2$. Let also $\{p_t\}_{t \geq 0}$ be a (smooth) solution of the Fokker-Planck equation with potential V and with initial datum p_0 . Then, there is a constant C depending on $D_{\text{KL}}(p_0\|q)$, $M_s(p_0)$, and s such that for all $t > 0$,*

$$D_{\text{KL}}(p_t\|e^{-V}) \leq \frac{C}{t^\kappa}, \quad \text{with } \kappa = \frac{1-2\delta}{\delta} = \frac{s-2}{2-\beta}. \quad (41)$$

where δ is given in equation 40.

Note that as $\beta \rightarrow 2$, one recovers the usual logarithmic Sobolev inequality as discussed in Sect. A.1. We summarize the said examples in the following table.

Table 3: Rate of convergence to equilibrium state $q \propto e^{-V}$ in KL divergence

Examples of $q \propto e^{-V}$	Rate of convergence in KL divergence
$q \propto e^{- x ^\beta}$, $\beta \geq 2$	at least $e^{-2\lambda t}$
Special case: $\mathcal{N}(0, \sigma)$	at least $e^{-2\lambda t}$, with $\lambda = \frac{1}{\sigma}$
$q \propto e^{- x ^\beta}$, $0 < \beta < 2$	$\mathcal{O}(t^{-\kappa})$, κ as in equation 41

B WEIGHTED POROUS MEDIUM EQUATIONS AND THEIR CONVERGENCE TO EQUILIBRIUM STATE

B.1 WEIGHTED POROUS MEDIUM EQUATION

The gradient flow of f -divergences for likelihood ratio. One may rewrite equation 33 in terms of the likelihood ratio denoted by h_t and defined as

$$h_t = \frac{dp_t}{dq} \quad (42)$$

By using the operator identity (q being the multiplication operator by the function q), i.e.

$$\nabla q = q(\nabla + \nabla \log q)$$

we have that

$$\nabla \cdot p_t \nabla f' \left(\frac{p_t}{q} \right) = q(\nabla + \nabla \log q) h_t \nabla f'(h_t)$$

and thus we can rewrite equation 33 as

$$\partial_t h_t = (\nabla + \nabla \log q) \cdot h_t \nabla f'(h_t) \quad (43)$$

Moreover if we denote ∇^* the adjoint of ∇ on $L^2(q)$ we have $\nabla^* = -(\nabla + \nabla \log q)$ and thus equation 43 has the form

$$\partial_t h_t = -\nabla^* h_t \nabla f'(h_t) \quad (44)$$

Let now $f_\alpha(x) = \frac{x^\alpha - 1}{\alpha(\alpha - 1)}$, we rewrite

$$h \nabla h^{\alpha-1} = \frac{1}{\beta} \nabla v^\beta = v^{\beta-1} \nabla v \implies v = h^{\alpha-1} \text{ and } h = v^{\beta-1} \implies \beta = \frac{\alpha}{\alpha-1}$$

and thus we obtain

$$\partial_t h_t = \frac{1}{\alpha} (\Delta + \nabla \log q \cdot \nabla) h_t^\alpha \quad (45)$$

for $t \geq 0$ and $x \in \mathbb{R}^d$ corresponding to a non-negative initial condition $h(x, 0) = h_0(x)$, $x \in \mathbb{R}^d$ is called weighted Porous Medium equation. For existence and uniqueness, see Dolbeault et al. (2008).

Remark B.1. The formula for f_α^* is given by

$$f_\alpha^*(y) = \begin{cases} \frac{(\alpha-1)^{\frac{\alpha}{\alpha-1}}}{\alpha} y^{\frac{\alpha}{\alpha-1}} \mathbf{1}_{y>0} + \frac{1}{\alpha(\alpha-1)} & , \alpha > 1 \\ \infty \mathbf{1}_{y \geq 0} + \left(\frac{1}{\alpha(1-\alpha)^{\frac{\alpha}{1-\alpha}}} |y|^{-\frac{\alpha}{1-\alpha}} \mathbf{1}_{y>0} - \frac{1}{\alpha(1-\alpha)} \right) \mathbf{1}_{y<0} & , \alpha \in (0, 1) \end{cases} \quad (46)$$

Remark B.2. For completeness, we discuss a related gradient flow known as *granular media equation*. To be precise, the 2-Wasserstein gradient flow of $\mathcal{F}(p) = \frac{1}{2} \text{MMD}[p, q]^2$ where $\text{MMD}[p, q]$ is the Maximum mean discrepancy (MMD) Gretton et al. (2012). By recalling equation 2, MMD is defined as

$$\text{MMD}[p, q] = \sup_{g \in \text{B}_{\text{RKHS}}(0,1)} \{E_Q[g] - E_P[g]\}$$

and its maximizer $\phi^*(z) = f_{q,p}(z) = \int k(x, z)q(x)dx - \int k(x, z)p(x)dx = k \star p(z) - k \star q(z)$ is called *witness function* between the probability densities q and p . In fact, g^* is the difference between the mean embeddings of q and p which finally makes MMD be re-written as the RKHS norm of the unnormalized g^* , i.e.

$$\text{MMD}[p, q] = \|\phi^*\|_{\mathcal{H}} \quad (47)$$

Then the gradient flow equation associated to \mathcal{F} leads to the granular media equation, i.e

$$\partial_t p_t(x) = \text{div}(p \nabla \cdot (k \star p - k \star q)) \equiv \text{div}(p_t \nabla \phi_t^*) \quad (48)$$

B.2 FUNCTIONAL INEQUALITIES FOR THE WEIGHTED POROUS MEDIUM EQUATION

In this section, we apply Theorem 4.5 in Dolbeault et al. (2008) to Weighted Porous Medium for the likelihood ratio $h_t = \frac{p_t}{q}$ and we prove polynomial decay in KL and χ^2 -divergence. Before we state the result we first define the L^r -Poincaré inequality and L^r -logarithmic Sobolev inequality (see also Dolbeault et al. (2008)).

Definition B.3. Let q be a probability measure on a Riemannian manifold (M, g) . Then the entropy is defined as follows: for any smooth function $f \in C^1(M)$

$$\mathbf{Ent}_q(f) := \int f \log \left(\frac{f}{\int f dq} \right) dq \quad (49)$$

while

$$\mathbf{Var}_q(f) := \int \left(f - \int f dq \right)^2 dq \quad (50)$$

Definition B.4. Let q be a probability measure on a Riemannian manifold (M, g) . Let also ν be a positive measure on (M, g) . We assume that $q \in (0, 1]$. We say that (q, ν) satisfies L^r -Poincaré inequality with constant C_P if and only if, for any nonnegative function $f \in C^1(M)$

$$[\mathbf{Var}_q(f^{2r})]^{1/r} \leq C_P \int |\nabla f|^2 d\nu \quad (51)$$

We say that (q, ν) satisfies L^r -logarithmic Sobolev inequality with constant C_{LS} if and only if, for any nonnegative function $f \in C^1(M)$

$$[\mathbf{Ent}_q(f^{2r})]^{1/r} \leq C_{\text{LS}} \int |\nabla f|^2 d\nu \quad (52)$$

Theorem B.5. If (q, q) satisfies a $L^{2/3}$ -Poincaré Sobolev inequality, for some constant $C_P > 0$, then for any non-negative initial condition $h_0 \equiv \frac{p_0}{q} \in L^2(q)$, we have for every $t \geq 0$

$$\chi^2(p_t \| q) \leq \left([\chi^2(p_0 \| q)]^{-1/2} + \frac{8}{9} C_P t \right)^{-2}. \quad (53)$$

Reciprocally, if the above inequality is satisfied for any g_0 , then (q, q) satisfies a $L^{2/3}$ -Poincaré Sobolev inequality with constant $C_P > 0$.

Table 4: Rate of convergence to equilibrium state $q \propto e^{-V}$ in χ^2 -divergence

Examples of $q \propto e^{-V}$	Rate of convergence in χ^2 divergence
$q = \frac{e^{- x ^\beta}}{2\Gamma(1+\frac{1}{\beta})}$, $0 < r \leq 1$, $1/2 \leq \beta < 1$	given in equation 53
$q = \frac{\beta}{(1+ x)^{1+\beta}}$, $1/2 \leq r < 1$, $\beta \geq \frac{2r}{1-r}$	given in equation 53

Theorem B.6. *Let $\alpha > 1$. If (q, q) satisfies a $L^{1/\alpha}$ -logarithmic Sobolev inequality, for some constant $C_{LS} > 0$, then for any non-negative initial condition h_0 such that $D_{\text{KL}}(p_0 \| q) < \infty$, we have for every $t \geq 0$*

$$D_{\text{KL}}(p_t \| q) \leq \left([D_{\text{KL}}(p_0 \| q)]^{1-\alpha} + \frac{4(\alpha-1)}{\alpha} C_{LS} t \right)^{-1/(\alpha-1)}. \quad (54)$$

Reciprocally, if the above inequality is satisfied for any g_0 , then (q, q) satisfies a $L^{1/\alpha}$ -logarithmic Sobolev inequality with constant $C_{LS} > 0$.

Next we discuss two examples of probability distributions satisfy L^r -Poincaré inequality and L^r -logarithmic Sobolev inequality:

Let $r \in (0, 1]$ and $\beta \in [\frac{1}{2}, 1)$. The probability measure

$$dq = \frac{1}{2\Gamma\left(1 + \frac{1}{\beta}\right)} e^{-|x|^\beta} dx, \quad x \in \mathbb{R} \quad (55)$$

satisfies a L^r -Poincaré inequality and L^r -logarithmic Sobolev inequality.

Let $r \in [1/2, 1)$, then for $\beta > \frac{2r}{1-r}$ the probability measure

$$dq = \frac{\beta}{(1+|x|)^{1+\beta}} dx, \quad x \in \mathbb{R} \quad (56)$$

satisfies a L^r -Poincaré inequality and a L^r -logarithmic Sobolev inequality.

C EXPERIMENTAL SETTING

Neural network architectures. We use the discriminator ϕ (compared to GAN setting) which is implemented using a neural network. In Table 5 we provide the architecture of the neural networks used to produce the experimental results. The Lipschitz constraint on ϕ is implemented by spectral normalization (the weight matrix in each layer of the D layers in total has spectral norm $\|W^l\|_2 = L^{1/D}$).

Mini-batch scheme. To handle larger data sets with $N > 200$ we use mini-batch training where we use, at each iteration step, N_{mb} randomly chosen data points from the target distribution to move N_{mb} particles. A proper choice of mini batch size N_{mb} should be chosen to learn the distribution as well as reduce the computation time. Default setting is $N_{\text{mb}} = 200$.

Data sets and important parameters. See Table 6. More details can be found in Supplementary material README.md.

Computational resources. Low dimensional examples 7.1 are computed in the tensorflow-CPU environment: *tensorflow-gpu=2.8.0 with CPU model Intel(R) Core(TM) i5-10210U CPU @ 1.60GHz ~ 2.11 GHz*. High dimensional examples D.1, 9, D.2 are computed in the tensorflow-GPU environment: *tensorflow-gpu=2.7.0 with GPU model Tesla K80 in Google cloud platform*.

CNN Discriminator	
5×5 Conv SN, 2×2 stride ($1 \rightarrow ch_1$)	leaky ReLU
	Dropout, rate 0.3
5×5 Conv SN, 2×2 stride ($ch_1 \rightarrow ch_2$)	leaky ReLU
	Dropout, rate 0.3
5×5 Conv SN, 2×2 stride ($ch_2 \rightarrow ch_3$)	leaky ReLU
	Dropout, rate 0.3
Flatten with dimension ℓ_3	
$W^4 \in \mathbb{R}^{\ell_3 \times d}$ with SN, $b^4 \in \mathbb{R}^d$	ReLU
$W^5 \in \mathbb{R}^{d \times 1}$ with SN, $b^5 \in \mathbb{R}$	Linear

(a) Image data (MNIST, CIFAR10)

FNN Discriminator	
$W^1 \in \mathbb{R}^{d \times \ell_1}$ with SN, $b^1 \in \mathbb{R}^{\ell_1}$	ReLU
$W^2 \in \mathbb{R}^{\ell_1 \times \ell_2}$ with SN, $b^2 \in \mathbb{R}^{\ell_2}$	ReLU
$W^3 \in \mathbb{R}^{\ell_2 \times \ell_3}$ with SN, $b^3 \in \mathbb{R}^{\ell_3}$	ReLU
$W^4 \in \mathbb{R}^{\ell_3 \times 1}$ with SN, $b^4 \in \mathbb{R}$	Linear

(b) Low dimensional data with dimension d Table 5: Neural network architectures of the discriminator $\phi : \mathbb{R}^d \rightarrow \mathbb{R}$

Dataset	f	L	data parameter	NN structure	learning rate	Δt	N_Q
2D t	KL, $\alpha = 2, 10$	1	$\nu = 0.5$	FFN (32, 32, 32)	0.01	0.1	200
Gene data	KL	1	$d = 2, 5, 10$ $d = 20, 50, 100$ $d = 200$	FFN (32, 32, 32) FFN (64, 64, 64) FFN (128, 128, 128)	0.1	5.0	245
MNIST	KL	1	conditioned	CNN (128, 128, 128)	0.05	1.0	200, 2K
MNIST	KL	1	$2 \rightarrow 0$ $d' = 64$ $d' = 128$	CNN (64, 64, 64) FNN (128, 256, 256) FNN (256, 512, 256)	0.01 0.01	0.1 0.1	200 200
2D Gaussian	KL	1, 10	$\sigma_Q = 2.0$	FFN (32, 32, 32)	0.05	1.0	200
2D $e^{- x ^\beta}$	KL $\alpha = 2$	1	$\beta = 0.4$	FFN (32, 32, 32)	0.05	0.1	200
CIFAR10	KL	1	label=0	CNN (128, 128, 128)	0.01	0.1	200
2D Gaussian Mixture	KL	1, 10, 100, None	$\sigma_Q = 0.5$	FFN (32, 32, 32)	0.005	1.0	200
12D Gaussian Mixture	KL	1	$\sigma_Q = 0.5$ $d' = 2$	FFN (32, 32, 32) FFN (32, 32, 32)	0.005	0.5 0.05	5K 200
2D 2 Gaussian Mixture	KL	1	$\sigma_Q = 1.0$ Mixing ratio $r = [0.8, 0.2]$	FFN (32, 32, 32)	0.005	1.0	200

Table 6: Data sets and important parameters

D ADDITIONAL EXPERIMENTS

D.1 ADDITIONAL HIGH DIMENSIONAL EXAMPLE

CIFAR10. We applied $(f_{\text{KL}}, \Gamma_1)$ generative particle algorithm and generated high dimensional image data. Using Lipschitz regularized KL -divergence, we transported samples from the *logistic distribution* P to samples from the target image *distribution for airplanes* Q . L is fixed to 1 through-

out as we found, empirically, that the algorithm is stable for this value and unstable for larger L (for example when $L = 10$ the algorithm diverges). Training data which are samples from the target distribution Q are described as: $N = 200$ number of color images whose pixels are in $[0, 1]^{32 \times 32 \times 3}$. On purpose, we used a small number of samples $N = 200$ which corresponds to 3.3% of the entire 60,000 data, to generate new images, see Figure 11.

Overall, we observe from our experiments that Lipschitz regularized particle methods generate realistic looking samples from a relatively small number of "real" samples from Q . We suspect that learning the empirical distribution of Q using generative particles allows us to approximate individual samples from Q see equation 16. In fact, our setting rigorously allows comparing non absolutely continuous empirical distributions while the particles are driven towards the empirical distribution of Q by the gradient flow, see equation 16.

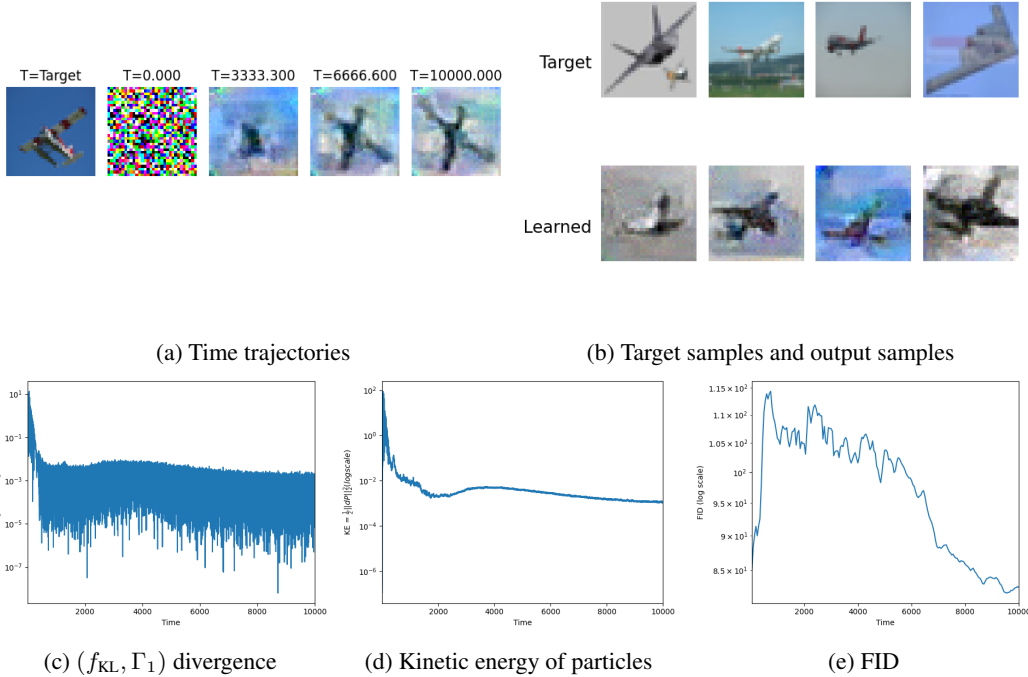


Figure 11: (CIFAR10, 200 Training samples) Generative particles algorithm on 2D images are less likely to meet with mode collapse even with small number of training data. (a) Time trajectories of (f_{KL}, Γ_1) -generative particle algorithm. Particles from the logistic distribution in the space $[0, 1]^{3072}$ are transported to the label 0 (airplane) data. (b) The generated samples vary in shape without mode collapse. (c) The particles are transported through the (f_{KL}, Γ_1) -flow. (d) Lipschitz regularized fisher information gives a more stable performance measure compared to the (f_{KL}, Γ_1) -divergence. (e) The final FID score is 82.61. Learning rates are chosen as $\gamma = 0.1, \delta = 0.01$.

D.2 ADDITIONAL LATENT GENERATIVE PARTICLES EXAMPLE

2D Mixture of Gaussians embedded in 12D (Revisited). The Figure 9 (b) shows that Lipschitz regularized generative particles algorithm struggles in making particles converge to the 2D plane where the mixture of Gaussians lies. It is interpreted that our algorithm produces noisy outputs compared to GANs. The main reason is for each step GPA minimizes $D_f^{\Gamma_L}(P||Q)$ using the first order explicit Euler method while GANs minimize $D_f^{\Gamma_L}(P||Q)$ by training a nonlinear generator g_{θ_t} . To make up for this behavior, we capture the sub-manifold (2D plane) from the latent space obtained by auto-encoders. Then our algorithm transports particles to capture the four wells. It is already shown in the Figure 8 that our algorithm performs well in this task. The key for the success of latent GPA is the Q -perfect encoding property in the Theorem 5.1. We compare the two Figures

12 and 13 where the latent spaces are obtained by training auto-encoders using different losses: the former uses Mean Square Error (MSE) in the real space, and the latter uses MSE in the real space regularized by KL divergence ($2 * \text{MSE} + \text{KL}$). The former auto-encoder is over-fitted and fails to achieve Q -perfect encoding property. In this case, the divergence converged in the latent space but the reconstructed outputs did not capture the four wells. However, the outputs from the latter captures the four wells in the 2D plane as well as the 10D orthogonal subspace.

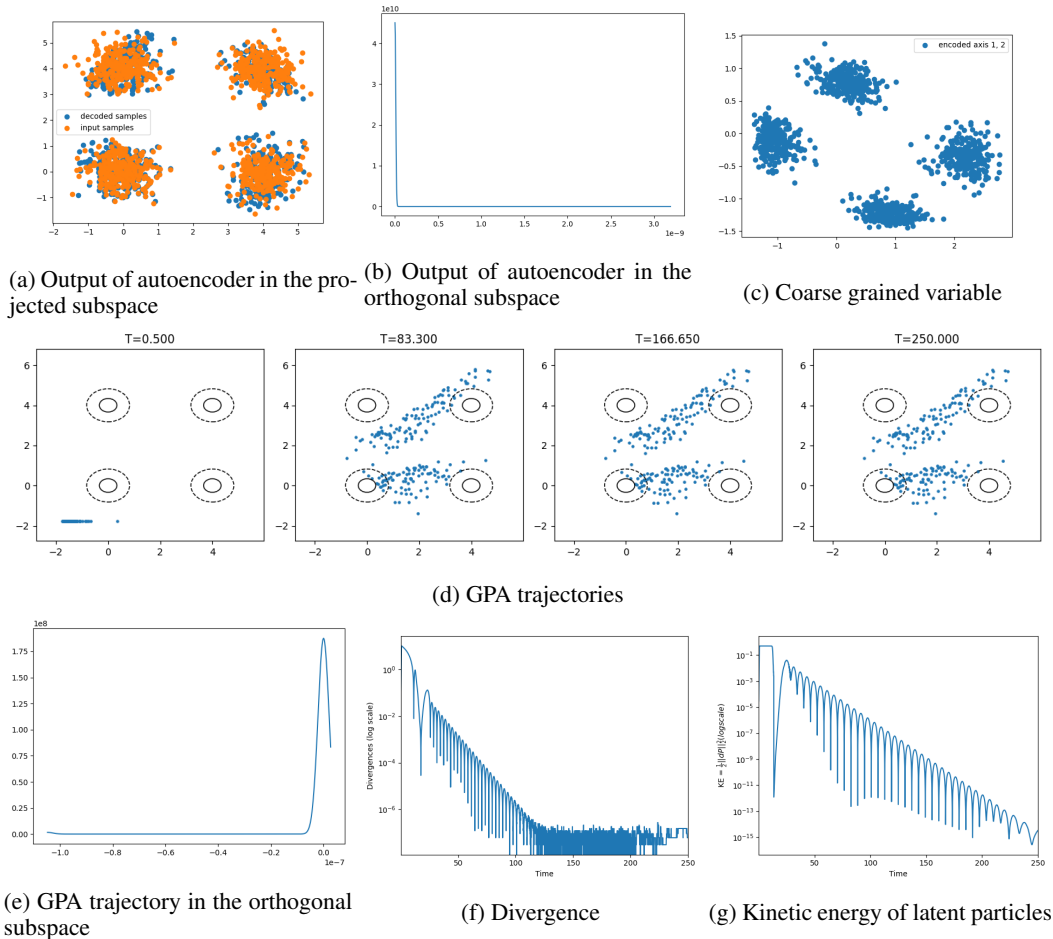


Figure 12: **(2D Mixture of Gaussians embedded in 12D, latent generative particles algorithm with latent dimension 2) Auto-encoder without Q -perfect encoding property.** The auto-encoder is trained using MSE loss and is over-fitted to the training samples. **(a)-(b)** The reconstructed outputs for the training samples of the auto-encoder. **(c)** The latent particles for the training samples of the auto-encoder. It captures the four wells. **(d)** Trajectories of reconstructed outputs from the latent generative particles algorithm in the 2D projected plane. The generated samples are unknown to the decoder. The reconstructed outputs fail to capture the four wells. **(e)** Final trajectory of the reconstructed outputs from the latent generative algorithm in the 10D orthogonal subspace. **(f)-(g)** Performance measures of particles transportation in the latent space. The source particles converges to the targets in the latent space. The learning rates are chosen as $\gamma = 1.0$, $\delta = 0.005$.

D.3 MICROARRAY GENE EXPRESSION DATA MERGING IN DIFFERENT LATENT DIMENSIONS d'

In Figures 14, 15, we show the resulting transported particles in the latent space for varying $d' = 2, 5, 10, 20, 50, 100, 200$ and the reconstructed real space.

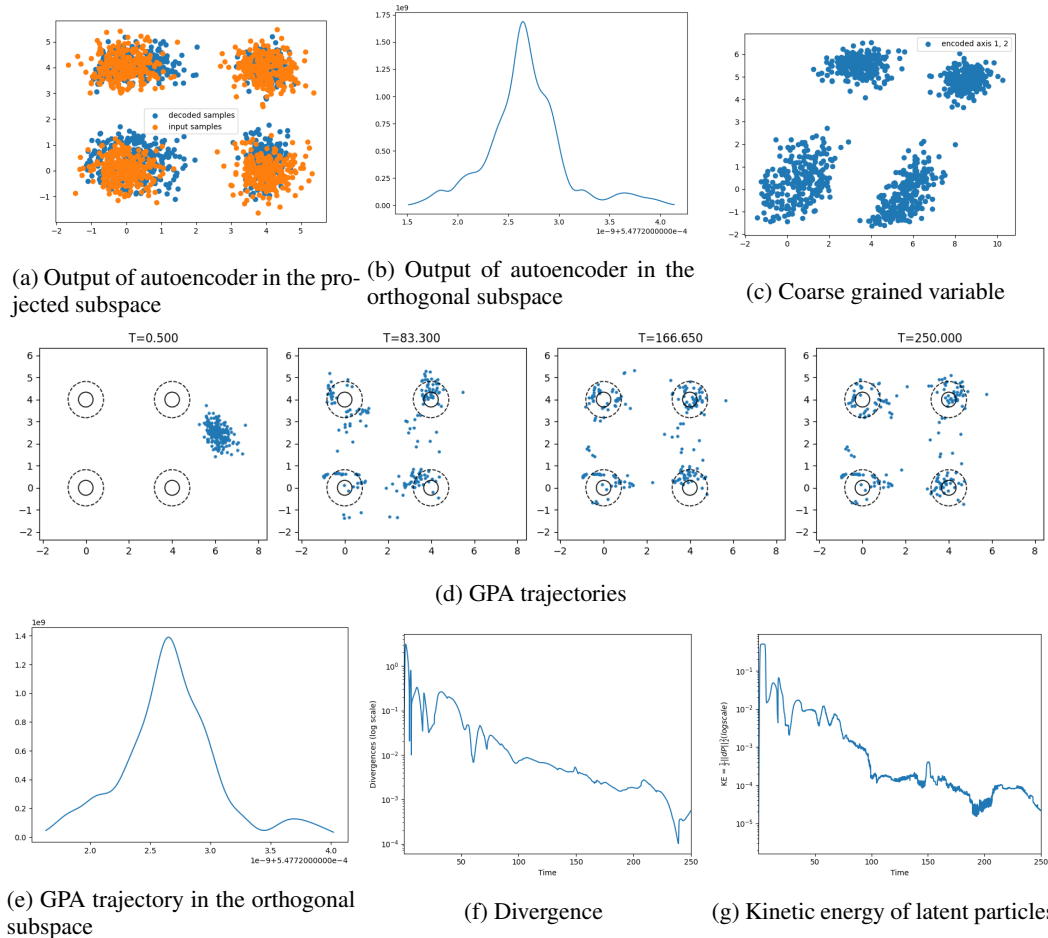


Figure 13: **(2D Mixture of Gaussians embedded in 12D, latent generative particles algorithm with latent dimension 2). Auto-encoder with Q -perfect encoding property.** The auto-encoder is trained using $2 * \text{MSE} + \text{KL}$ loss and reconstructs the target Q in an almost perfect manner. **(a)-(b)** The reconstructed outputs for the training samples of the auto-encoder. **(c)** The latent particles for the training samples of the auto-encoder. It captures the four wells. **(d)** Trajectories of reconstructed outputs from the latent generative particles algorithm in the 2D projected plane. The generated samples are unknown to the decoder. The reconstructed outputs captures the four wells. **(e)** Final trajectory of the reconstructed outputs from the latent generative algorithm in the 10D orthogonal subspace which are highly concentrated to 0. The problematic behavior from the original generative particles algorithm (See Figure 9) is settled. **(f)-(g)** Performance measures of particles transportation in the latent space. The source particles converges to the targets in the latent space. The learning rates are chosen as $\gamma = 1.0, \delta = 0.005$.

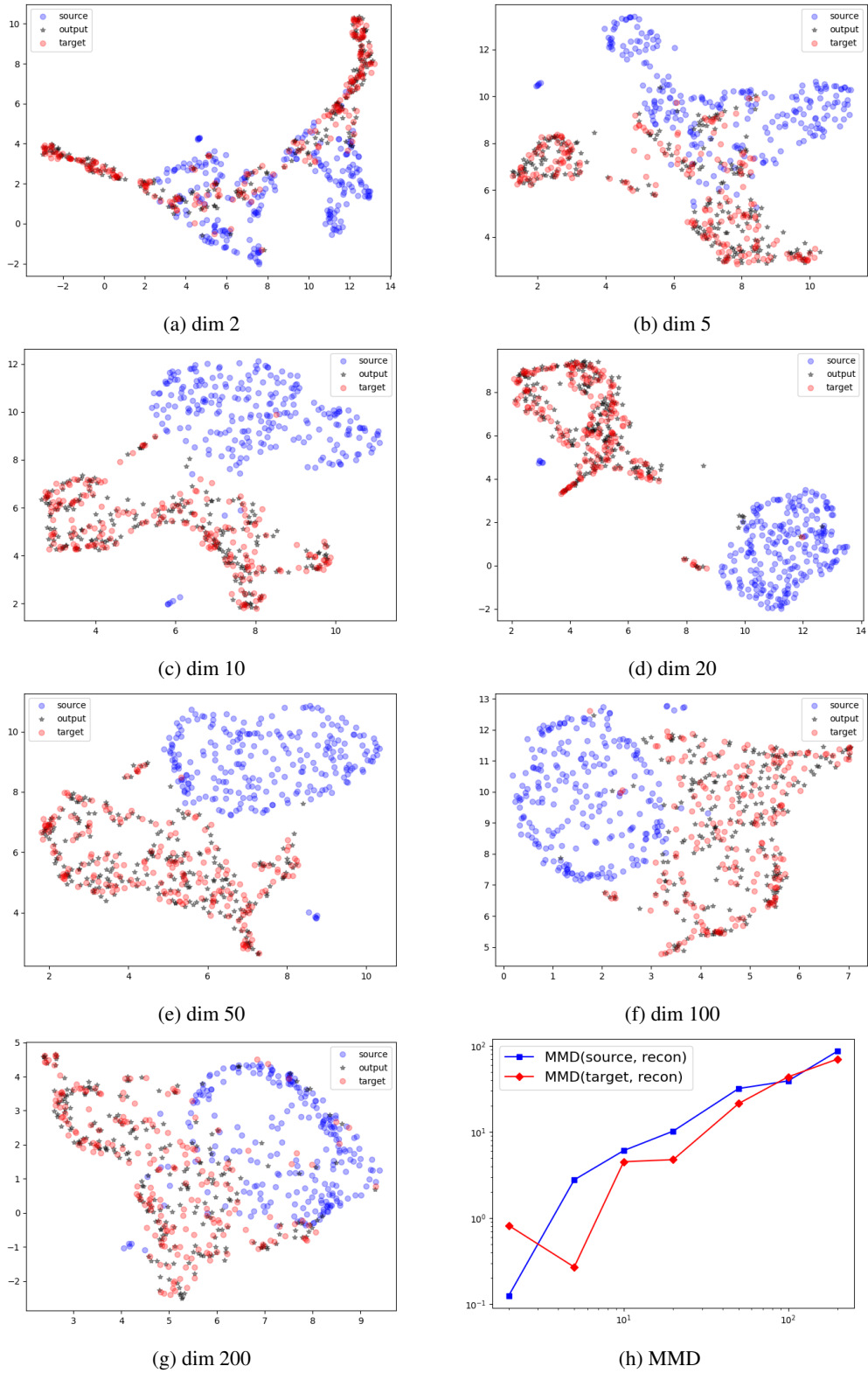


Figure 14: (Gene expression data, BreastCancer) Latent samples. **blue: source, red: target, black: transported.** (h) The distance between the latent distributions. **blue: $MMD(P_0^Z, P_T^Z)$, red: $MMD(Q^Z, P_T^Z)$, black: $MMD(P_0^Z, Q^Z)$** with $T = 25,000$.

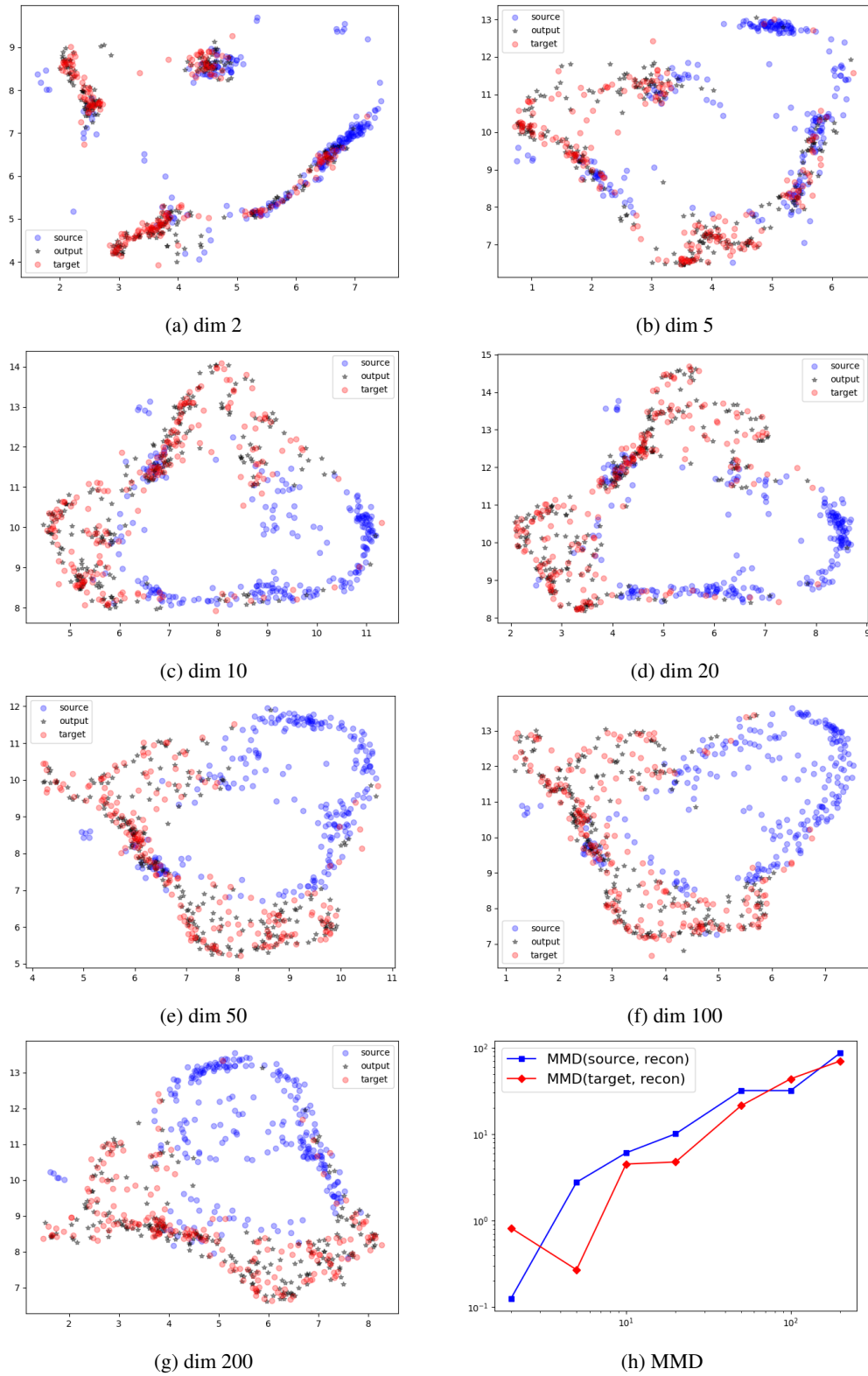


Figure 15: (Gene expression data, BreastCancer) Reconstructed samples. **blue: source, red: target, black: transported.** (h) The distance between the reconstructed distributions. **blue: $\text{MMD}(P_0^y, P_T^y)$, red: $\text{MMD}(Q^y, P_T^y)$, black: $\text{MMD}(P_0^y, Q^y)$** with $T = 25,000$.